Root zone of the sheeted dike complex in the Oman ophiolite

Adolphe Nicolas, Françoise Boudier, J. Koepke, Lyderic France, Benoit Ildefonse, C. Mevel

Geochemistry Geophysics Geosystems G3
AN ELECTRONIC JOURNAL OF THE EARTH SCIENCES
Published by AGU and the Geochemical Society

Article
Volume 9, Number 5
2 May 2008
Q05001, doi:10.1029/2007GC001918
ISSN: 1525-2027

Root zone of the sheeted dike complex in the Oman ophiolite

Adolphe Nicolas and Françoise Boudier
Géosciences Montpellier, CNRS, Université Montpellier 2, CC60, F-34095 Montpellier Cédex 05, France (francoise.boudier@gm.univ-montp2.fr)

Jurgen Koepke
Institut für Mineralogie, Leibniz Universität Hannover, Callinstrasse 3, D-30167 Hannover, Germany

Lydéric France and Benoît Ildefonse
Géosciences Montpellier, CNRS, Université Montpellier 2, CC60, F-34095 Montpellier Cédex 05, France

Catherine Mevel
Géosciences Marines, IPG, CNRS, 4 Place Jussieu, F-75252 Paris Cédex 05, France

[1] In the Oman ophiolite crustal section, a contact zone between the gabbro unit and the volcanics and diabase sheeted dikes, called the root zone of the sheeted dike complex, has been recently mapped at a fine scale in a selected area. The Oman ophiolite is derived from a fast spreading ridge which had a melt lens located between the main gabbro unit and the root zone of the sheeted dike complex. With a few exceptions accounted for, this horizon has a fairly constant thickness, ~100 m, and a crude internal pseudo-stratigraphy. At the base of the root zone are isotropic ophitic gabbros interpreted as a thermal boundary layer. This layer is transitional between the magmatic system of the melt lens, convecting at 1200°C, and a high-temperature (<1100°C) hydrothermal system, convecting within the root zone. Above this level, the isotropic gabbros have been, locally, largely molten due to an influx of seawater, at ~1100°C, thus generating varitextured ophitic and pegmatitic gabbros. These latter gabbros constitute the upper part of the root zone and are associated with trondjhemitic intrusions as screens in the lower sheeted dikes. Diorites and trondjhemites were also generated by hydrous melting, at temperatures below 1000°C. The whole root zone is a domain of very sharp average thermal gradient (~7°C/m). At the top of the root zone, a new thermal boundary layer, with diabase dikes hydrated in amphibolite facies conditions, separates the preceding high-temperature convective system from the well-known greenschist facies (<450°C) hydrothermal system operating throughout the sheeted dike complex, up to the seafloor. The isotropic gabbros near the base of the root zone are intruded by protodikes with distinctive microgranular margins and an ophitic center. Protodike swarms are exceptional because, intruding a medium at ~1100°C, they are largely destroyed by dike-in-dike intrusions and by hydrous melting. However, they demonstrate that this zone was generated by melt conduits issued from the underlying melt lens. Each dike of the sheeted dike complex is thus fed by one protodike. As this zone has been recently drilled by IODP in the eastern Pacific Ocean, a brief comparison is proposed.

Components: 13,629 words, 15 figures, 2 tables.

Keywords: fast spreading ridges; lid/gabbros transition; Oman ophiolite; HT hydrothermalism.

Index Terms: 8140 Tectonophysics: Ophiolites (3042); 8135 Tectonophysics: Hydrothermal systems (0450, 1034, 3017, 3616, 4832, 8424); 3614 Mineralogy and Petrology: Mid-oceanic ridge processes (1032, 8416).

Received 1 December 2007; **Revised** 13 February 2008; **Accepted** 12 March 2008; **Published** 2 May 2008.

Nicolas, A., F. Boudier, J. Koepke, L. France, B. Ildefonse, and C. Mevel (2008), Root zone of the sheeted dike complex in the Oman ophiolite, *Geochem. Geophys. Geosyst.*, *9*, Q05001, doi:10.1029/2007GC001918.

1. Introduction

[2] A small melt lens has been imaged by multichannel seismic profiles in the late 1980s below fast spreading centers, extending <1 to 4 km on each side of the ridge axis and locally as thin as 30 m [e.g., *Detrick et al.*, 1987; *Harding et al.*, 1989; *Collier and Singh*, 1997; *Singh et al.*, 1998, 2006; *Kent et al.*, 2000]. This discovery has raised the question of how this lens relates to the overlying sheeted dike complex, as previously described from oceanic drilling [e.g., *Alt et al.*, 1993, 1996; *Bach et al.*, 2003] and in tectonic windows such as Hess Deep [*Karson et al.*, 1992, 2002b] and fracture zones [e.g., *Juteau et al.*, 1995; *Karson et al.*, 2002a]. The recent IODP hole in the eastern Pacific Ocean in Hole 1256D [*Wilson et al.*, 2006], has penetrated, at 1400 m below seafloor, 100 m of gabbros at the base of the sheeted dike complex. It is not certain that the last cored gabbros have attained the level of the former melt lens and represent the top of the gabbro unit. On the basis of field studies in Oman, we will propose criteria to distinguish gabbros which have settled on the floor of the former melt lens from gabbros crystallized at and above its roof. This zone between the base of the sheeted dikes and the top of the gabbro unit is called herein the root zone of the sheeted dike complex (RZSDC).

[3] The RZSDC has recently raised interest with petrological studies in Cyprus [*Gillis and Roberts*, 1999; *Gillis*, 2002; *Gillis and Coogan*, 2002] and in Oman [*MacLeod and Yaouancq*, 2000], following earlier descriptions of the RZSCD by *Pallister and Hopson* [1981] and *Rothery* [1983]. More general studies have been conducted by *Coogan et al.* [2003] and in Oman ophiolite, by *MacLeod and Rothery* [1992] and by *Nicolas and Boudier* [1991], whose comprehensive structural study is expanded here. General descriptions regard the RZSDC as a thin and complex assemblage of hydrous gabbros and more acidic, plutonic bodies, increasingly intruded upsection by diabase dikes, thus grading into the sheeted dike complex. In some studies, this zone has been ascribed to the final stage of the magmatic differentiation of the gabbro unit. This differentiation would occur at the top of a magma chamber, in the presence of residual water of deep origin. The RZSCD has also been regarded as originating at and above the melt lens roof as a thermal boundary layer between two main convective systems: below, the melt lens filled with a basaltic magma at ~1200°C, and above, the diabase sheeted dike complex and associated volcanics which are cooled by seawater hydrothermal cells [*Nicolas and Boudier*, 1991; *Chenevez and Nicolas*, 1997; *Gillis and Roberts*, 1999]. We depart here from our former interpretation, by introducing a new hydrothermal convection system, operating at very high temperature between the two systems mentioned above.

[4] We regard the well-known hydrothermal system [e.g., *Nehlig et al.*, 1994; *Alt et al.*, 1996] as low temperature (LT, up to 400–450°C), because it is shown below that the RZSDC, when it was active above the melt lens, was altered by a high temperature (HT > 400–450°C) hydrothermal system, just as the gabbro unit located below [*Manning et al.*, 1996; *Nicolas et al.*, 2003; *Bosch et al.*, 2004]. The LT hydrothermal cells close at a depth of ~1–2 km, at the base of the sheeted dike complex.

[5] Considering the renewed interest in this zone arising from the recent drilling of IODP Hole 1256D [*Wilson et al.*, 2006], it seemed appropriate to revisit our 1991 study in Oman ophiolite, incorporating it in a new detailed map. This ophiolite is both very large with magnificent outcrops, and inferred to be derived from a fast spreading oceanic ridge [*Nicolas et al.*, 2000], where melt lenses are actually inferred from seismic-velocity inversions. This study is focused on a limited area in the Sumail Massif, which is located in the southern part of the belt where our mapping is more detailed. In this area, all units from the lavas to the Moho are parallel and gently tilted, in contrast with domains affected by ridge segmentation, as briefly recalled below. Petrostructural descriptions from a few tens of sites from other massifs studied during the structural mapping of the Oman ophiolite show that RZSCD in this ophiolite generally have many common features throughout the belt [*Nicolas et al.*, 2000]. However, significant differences are noted depending on

whether the RZSDC belong to a domain affected by ridge segmentation or not. The results presented here on RZSDC should apply to ocean ridges spreading in steady state conditions, but we will briefly envisage how RZSDC would be modified in situations affected by ridge segmentation.

[6] Finally, as a word of caution, it should be stressed that RZSCD are complex interface zones where several processes have been active at different times. In particular, field observations are the end product of superimposed processes initiated above the melt lens and continued off-axis on a few tens of kilometers.

2. Choice of the Studied Area

[7] Magmatic intrusions are observed in a number of RZSDC in the Oman ophiolite. They were mapped as "late intrusive" [*Lippard et al.*, 1986; *Ministry of Petroleum and Minerals*, 1986], encompassing, wehrlites and gabbronorites, uralitic gabbros, diorites and tronjhemites, the last one making up magmatic breccias with diabase dikes. Olivine gabbros have not been reported among these intrusions These "late intrusive" have been related to domains where accretion was under the influence of major tectonic and magmatic activity related to ridge propagation [*Juteau et al.*, 1988; *MacLeod and Rothery*, 1992; *Nicolas and Boudier*, 1995; *Boudier et al.*, 2000; *Adachi and Miyashita*, 2003; *Miyashita et al.*, 2003; *Umino et al.*, 2003]. Here, they are referred to as domains of "ridge segmentation" and opposed to domains where the accretion should have been steady state, called here "normal" domains, considering their continuity and homogeneity. To better identify and estimate the fraction of the Oman ophiolite affected by ridge segmentation we used, as first criterion, the occurrence of gabbronorite and large diorite-trondjhemite bodies; both are, without ambiguity, late intrusions in RZSDC and they have been attributed to hydrated magmas [*Boudier et al.*, 2000]. However, trondjhemites are also present, as small bodies, in domains away from segmented areas. Consequently, only the bodies larger than 1 km in extension were considered to define the domains of ridge segmentation. With these criteria, we have estimated, from the geological map of northern Oman at a scale of 1/250,000 [*Ministry of Petroleum and Minerals*, 1992], that the total surface fraction of gabbro areas affected in Oman ophiolite by these large intrusions is 47% versus 53% of "normal" gabbro areas.

[8] Our field study is located in the Sumail massif, one of the southern massifs in the Oman ophiolite where the effects of ridge segmentation are minor (Figure 1). This very large and flat-bottomed synform has been mapped with the highest density of field stations during the systematic structural mapping in this ophiolite, over the last 25 years. The general structure of the ophiolite is dominated by a central, NW-SE trending system which was opened inside a NE-SW trending external domain [*Nicolas and Boudier*, 1995; *Nicolas et al.*, 2000]. The large NW-SE ridge segment extends in the Nakhl and Haylayn massifs to the NW, and in the Wadi Tayin massif to the SE. It is subdivided in individual segments which are centered on a few mantle diapirs.

[9] The area considered here is located between Samrah oasis and Wadi Abda (Figures 1 and 2). This oceanic crust was generated by the NW-SE trending spreading center of Maqsad [e.g., *Jousselin et al.*, 1998].

3. Main Petrostructural Units in the Mapped Area

[10] The map in Figure 2 is based on ~100 main field stations, each one generally covering small cross sections or a few sites of individual measurements. The map also integrates a few geological limits from the geological map of Oman at the 1:100,000 scale [*Ministry of Petroleum and Minerals*, 1986]. For mapping purposes, the following operational units, from top to bottom of the ophiolitic sequence, are retained (see cross section in Figure 2): 1, lavas; 2, sheeted dike complex; 3, RZSDC; and 4, main gabbro unit represented at this level by the uppermost foliated gabbros. The RZSDC lower limit with these foliated gabbros is remarkably sharp, generally marked by a discordance (Figure 2). Its upper boundary is traced where the diabase dikes fraction attains ~90%. These unit boundaries depart only marginally from those of *Nicolas and Boudier* [1991].

3.1. Lavas

[11] Lavas crop out close to Wadi Abda (Figure 2a) and in a small area. In Wadi Abda, lava flows have an orientation of 95S25°, with some dispersion; they are conformable with the underlying sheeted dike unit. As this locality is close to the eastern limit of the Sumail synform, next to an extrusion of the underlying Hawasina sedimentary units, the

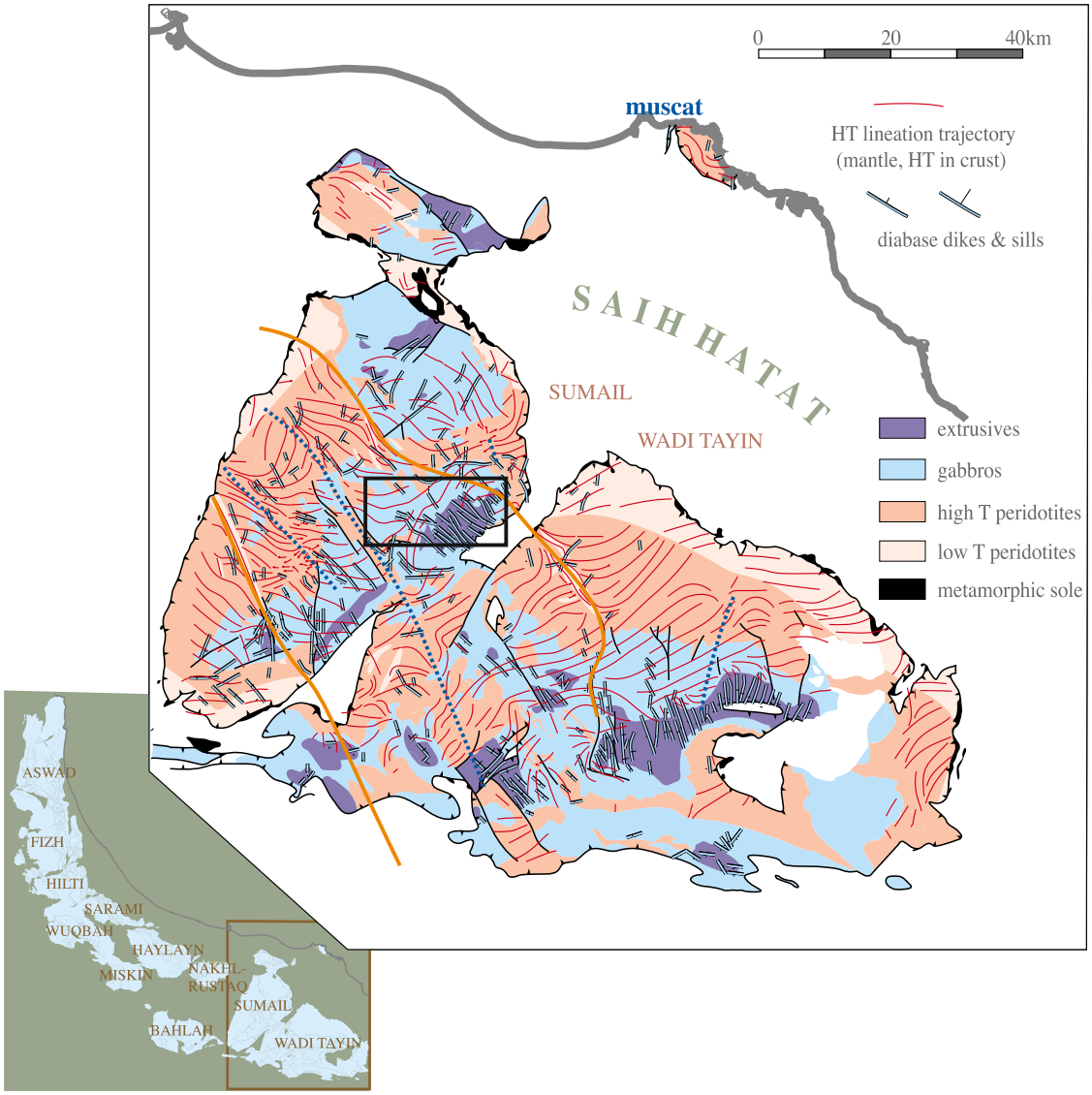

Figure 1. Simplified geological and structural map of Sumail and Wadi Tayin massifs, and location in the Oman ophiolite [after *Nicolas et al.*, 2000]. The black rectangle shows the location of the map in Figure 2. Blue dotted lines are inferred ridge axes, and yellow lines are limits of the large NW-SE segment opened in a NE-SW ridge system.

lava flows may have been locally tilted with respect to more internal units.

3.2. Sheeted Dikes

[12] This unit is composed of parallel, ~1 m thick, diabase dikes, bounded by dark and very fine-grained chilled margins. Older dikes are commonly larger, and seem to be more altered by hydrothermal fluids, grading into epidosites and bounded by epidote-rich veins. Younger dikes are thinner, black and less altered. Average field orientations at each measurement station are based on 10 to 50 individual chilled margins measurements.

[13] In the deepest diabase dikes (2b in cross section, Figure 2), chilled margins are less conspicuous and internal texture is coarser (0.1–0.2 mm) than in the dikes above (2a, Figure 2). They are little affected by greenschist facies, LT, hydrothermal alteration and display, with a brown hornblende an amphibolite, HT, metamorphism (Figure 3a).

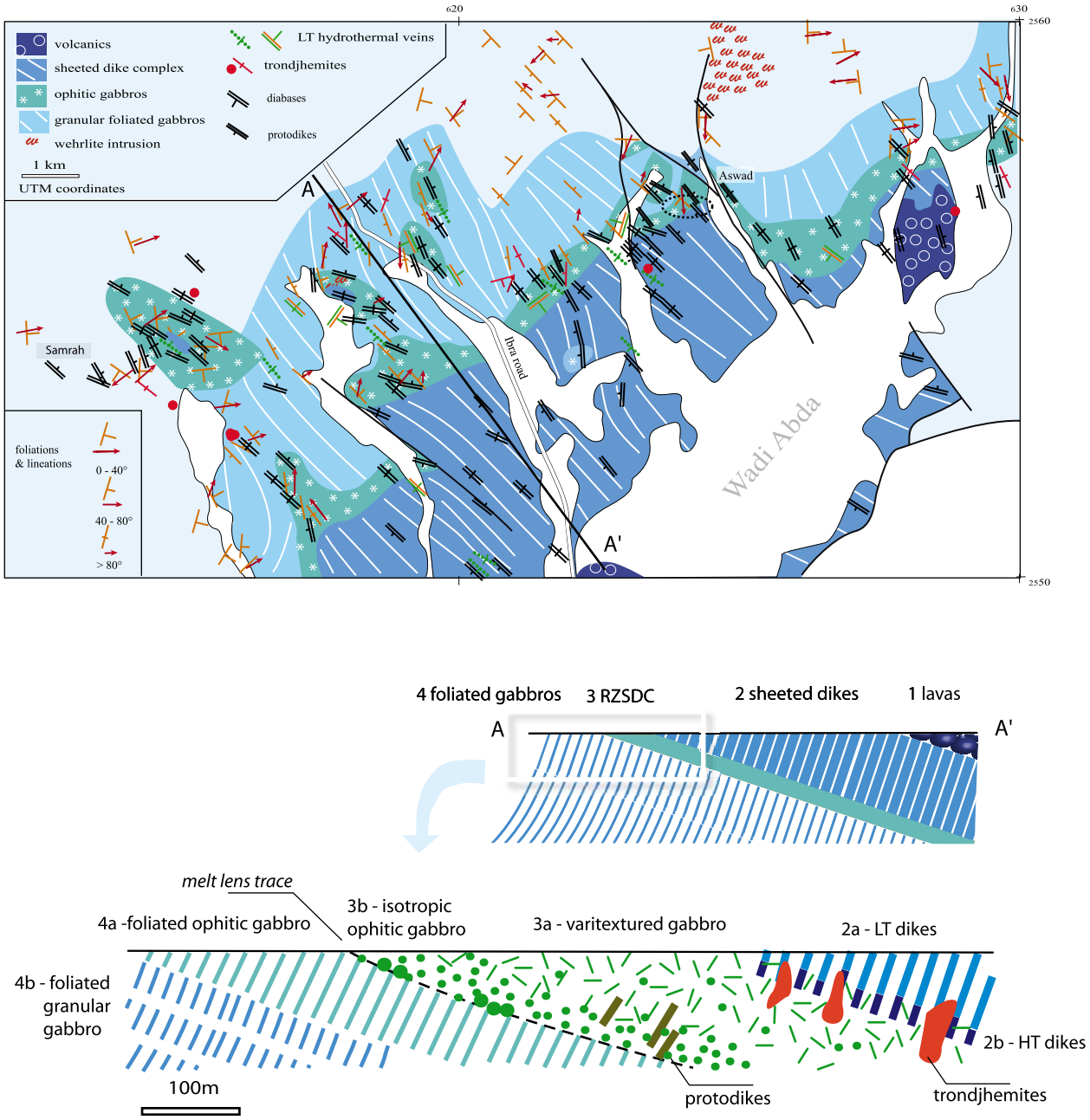

Figure 2. Map and cross section in the upper ophiolite units, from Samrah to Wadi Abda (Sumail massif) (location in Figure 1). Dotted ellipse is Wadi Gaz location. The upper cross section, along the A-A′ profile in map, locates the main units, and the lower cross section (box in the upper section) illustrates the RZSDC structure and petrology.

3.3. Root Zone of the Sheeted Dike Complex

[14] Gabbroic rocks in this critical zone are isotropic (3b in cross section, Figure 2) and varitextured gabbros (3a, Figure 2), characterized by an ophitic texture, where the meshes between the network of plagioclase laths are filled by clinopyroxene oikocrysts, usually altered to hornblende, and olivine grains which usually are totally altered (Figures 3b and 3c). Collectively, we refer to these rocks as "ophitic gabbros."

[15] A crude order of superimposition and relative chronology within the RZSDC can be established from the relations between different ophitic gabbros and other related facies described below, pointing to a decrease of temperature with time. In

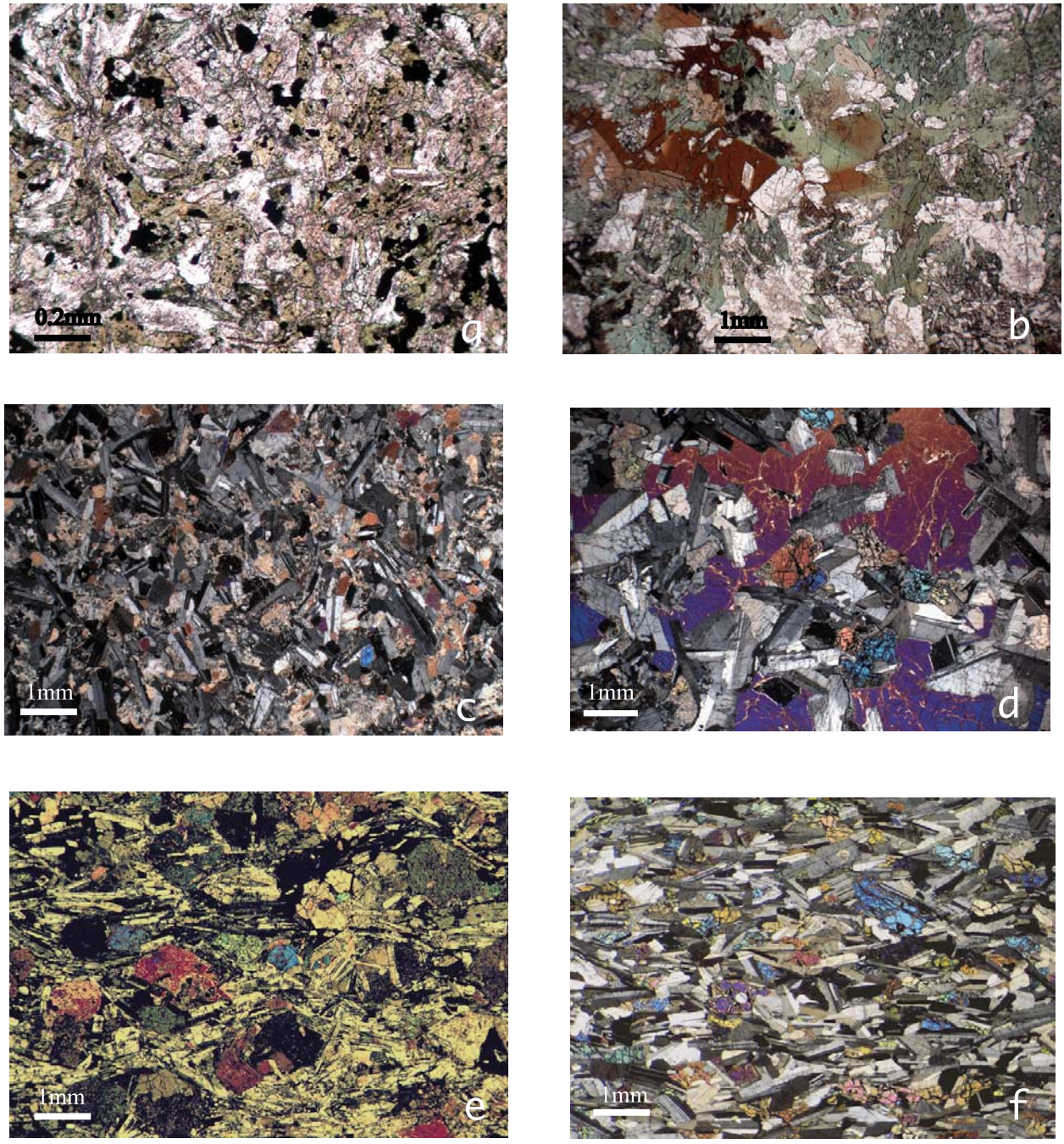

Figure 3. Microphotographs of (a) lowermost HT diabase dike from the sheeted dike complex, characterized by a medium-grained texture and brown hornblende (06OA-31k), (b) varitextured ophitic gabbro where clinopyroxene has been totally replaced by brown and green amphibole (06OA-20a), (c) fine-grained isotropic ophitic gabbro with interstitial brown hornblende and clinopyroxenes altered in green hornblende (OM06-25), (e) dry to nearly dry coarse-grained isotropic ophitic gabbro from the base of the RZSDC in which olivine presents a thin rim of HT hydrous alteration (06OA-2), (e) foliated, ophitic gabbro with plagioclase laths molded around subhedral clinopyroxene, from a few meters below the RZSDC, and (f) foliated granular upper gabbro from the gabbro unit (OM06-17).

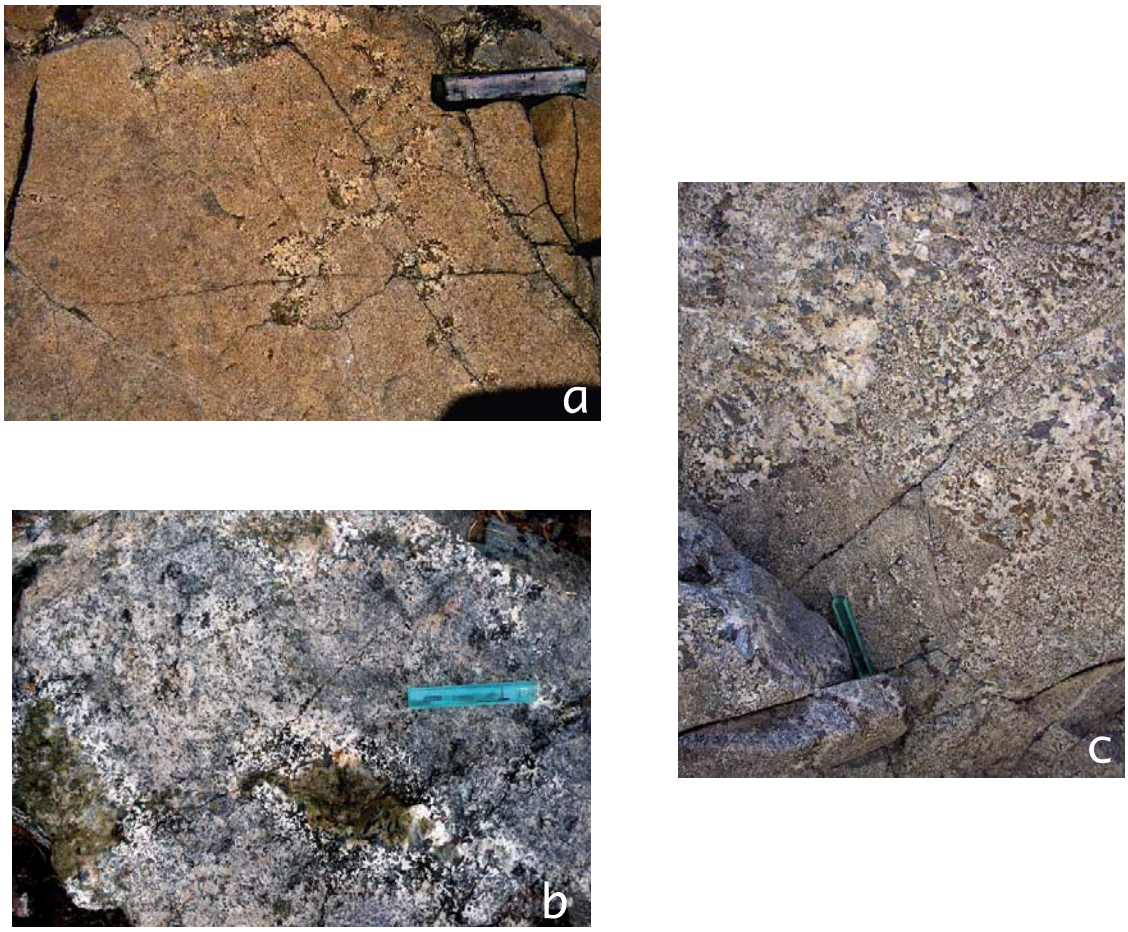

Figure 4. Facies of varitextured gabbros (scale bar is 10 cm). (a) Isotropic ophitic gabbro evolving in varitextured gabbro within nests of pegmatitic recrystallization (06OA20). (b) Varitextured ophitic gabbro with nests of LT (greenschist facies) crystallization with epidote-rich cores, indicative of an evolution ending with an episode of "autometamorphism" (06OA23). (c) Varitextured and pegmatitic ophitic gabbro with rooting of a pegmatitic dike (05OA17).

this respect, it is critical to integrate the results on a HT seawater alteration, ubiquitously present in the main gabbro unit [*Gregory and Taylor*, 1981; *Stakes and Taylor*, 1992; *Manning et al.*, 2000; *Nicolas et al.*, 2003; *Bosch et al.*, 2004]. Mineral assemblages resulting from HT ($\leq$1000°C) reactions described in the gabbro unit are also recorded in the RZSDC, with generally a complete HT alteration of olivine in a mixture of pale hornblende and chlorite, and of clinopyroxene in brown hornblende. The $\geq$1000°C hydrous reactions that develop orthopyroxene are not common in the RZSDC described here, in contrast with areas related to ridge segmentation [*Boudier et al.*, 2000].

[16] At the base of the RZSDC, just above the foliated gabbros described below, locally, restricted gabbro outcrops present a coarser isotropic ophitic texture, where olivine is still present in stocky crystals together with disordered plagioclase laths (plagioclase is also present in olivine as minute inclusions)(larger green dots in cross section, Figure 2). The meshes within the plagioclase framework are occupied by poikilitic clinopyroxene and opaque minerals (Figure 3d). Such gabbros have only a limited HT hydrous alteration, following the terminology defined by *Bosch et al.* [2004] in the main gabbro unit. In order to distinguish them from the overlying ophitic gabbros, we call them the dry ophitic gabbros. The transition from this thin horizon of mildly or no hydrated gabbros to the largely hydrated, overlying ophitic gabbros can be traced in the field. Small hills with reddish, weathered blocks of dry ophitic gabbros and underlying granular gabbros contrast with more grayish low lands formed by hydrated ophitic gabbros.

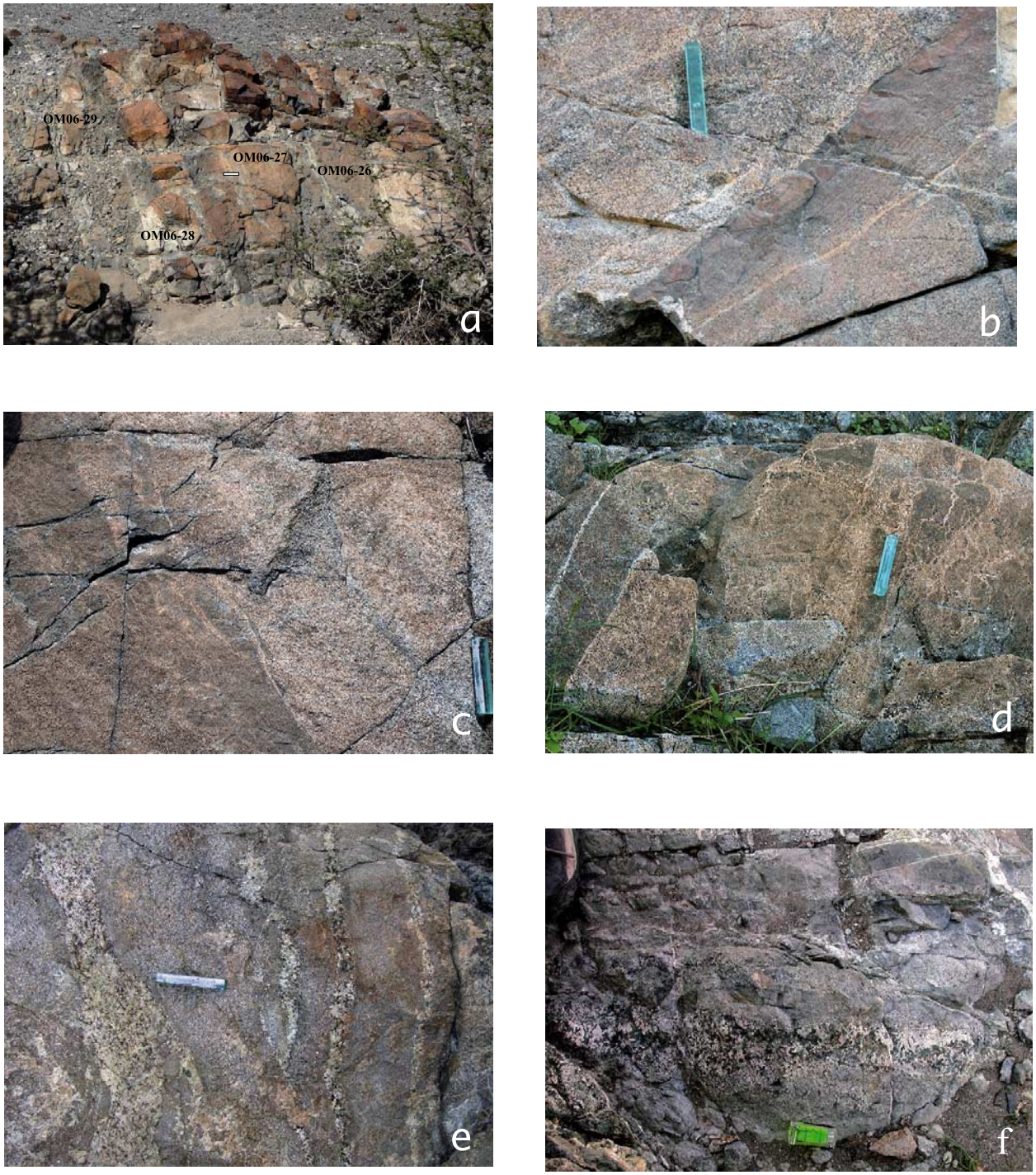

Figure 5. Diabase protodikes (scale bar is 10 cm). (a) Swarm of protodikes and dioritic intrusions (outcrop 06OA31, with reference to microprobe analysis sampling). (b) Sliver of a protodike with its microgranular margin intruding an ophitic gabbro (top, left) and grading internally into an ophitic gabbro (89OA101). (c and d) Same outcrop as Figure 5b, showing in Figure 5c a dark and fine-grained protodike margins and in Figure 5d a brecciated protodike, both being dismembered and assimilated by a gabbroic matrix. (e and f) HT pegmatitic gabbro dikes crosscutting protodikes (06OA2) (scale bar in Figure 5f is 3 cm).

[17] Isotropic ophitic gabbros may recrystallize in varitextured, locally, pegmatitic gabbros (Figure 4). In the varitextured gabbros, olivine is totally altered; clinopyroxene oikocrysts are largely or totally replaced by a brown hornblende grading into greenish hornblende (Figure 3b). In the field, pegmatitic varitextured gabbros are found as veins and inside circular patches, some 10 cm across, with dark green amphibole at the margin, whitish plagioclase in between and, commonly, epidote in the center (Figure 4b). Pegmatitic gabbros intrusions are either parallel to the sheeted dikes or flat-lying sills (Figure 4c).

[18] Diorites and trondjhemites occur as later intrusions of restricted size in the studied area, but can be hundreds of meters in segmentation-related areas. Trondjhemites are located close to, or within, the sheeted dike complex, commonly making up the dominant screen in the transition zone to the 100% sheeted dike unit. Trondjhemites are also observed in magmatic, brecciated dikes and sills in which they constitute the matrix surrounding corroded diabase fragments.

3.4. Protodikes With Microgranular Margins

[19] *Nicolas and Boudier* [1991] described "diabase protodikes" in the Oman RZSDC. They differ from other diabase dikes by their microgranular versus chilled margins and by a coarser and occasionally fluidal, ophitic texture, slightly different in this respect from their ophitic gabbros country rocks. When the protodikes are not brecciated, their orientations are within 10–20° to those of sheeted dikes (Figure 8). They can be isolated or mutually intrusive as in any dike swarm (Figure 5a), but most commonly, they are dispersed in an ophitic gabbro matrix. Protodike margin texture is microgranular and mosaic-shaped, with stocky plagioclase (Figure 6a). An anomalous concentration in opaque phases is locally noted in these fine-grained margins. Although hardly visible in thin section, protodikes contain a good preferred crystallographic orientation parallel to that of the dike, thus recording upward magmatic flow (Figures 6a and 6b). This fabric concerns mainly plagioclase, and is stronger in the microgranular margins (Figure 6a) than in the center (Figure 6b). In contrast with protodike cores which vanish into their ophitic gabbro matrix, the microgranular margins are very symptomatic because they survive to dike-in-dike intrusions, either as thin lenses inducing a fluidal aspect to (Figures 5b and 5c), or as blocks in magmatic breccias (Figure 5d). Orthopyroxene occurrence in the microgranular margins of protodikes is uncommon and restricted to some localities.

[20] Protodikes are usually emplaced in isotropic ophitic gabbros. They are, in turn, intruded by varitextured pegmatitic gabbros (Figures 5e and 5f). This demonstrates that their intrusion commonly occurred in the RZSDC after crystallization of the isotropic gabbros but before that of the varitextured gabbros. However, there is a continuum between protodikes and the LT diabase dikes with typical chilled margins. Some basaltic dikes are devoid of chilled margins and are coarser-grained in their center. The presence of diabase protodikes with their typical microgranular margins can be considered as a specific attribute of RZSDC. Finally, it should be mentioned that the microgranular texture is similar to that observed in microgabbronorites in the granular gabbros where they form lenses parallel to the gabbro layering (see below).

3.5. Foliated, Ophitic, and Granular Gabbros

[21] The base of the RZSDC is locally difficult to identify, despite the fact that it is a sharp discordance between overlying isotropic, ophitic gabbros and underneath foliated, ophitic gabbros (4a in cross section, Figure 2). Their foliation is magmatic (Figure 3e) commonly underlined by anorthosite layers. Foliation and layering are parallel to the general trend of the overlying sheeted complex and the associated lineation is steep. In the field, foliation and layering are commonly obliterated by large and irregular zones of recrystallized gabbros which had been ascribed to hydrous partial melting triggered by seawater intrusion at the wall of the magma chamber below the melt lens [*Nicolas et al.*, 2003; *Bosch et al.*, 2004] (Figure 4).

[22] Downward, the foliated, ophitic gabbros grade into the gabbro unit, through the foliated, granular gabbros (4b, Figure 2). Their texture is dominated by preferentially oriented tabular plagioclase laths, defining a strong magmatic foliation, together with elongated olivine aggregates and more stocky clinopyroxene grains (Figure 3f).

[23] In both the foliated, ophitic and granular gabbros, the layering is generally absent, or defined by anorthosite and microgabbro lenses, usu-

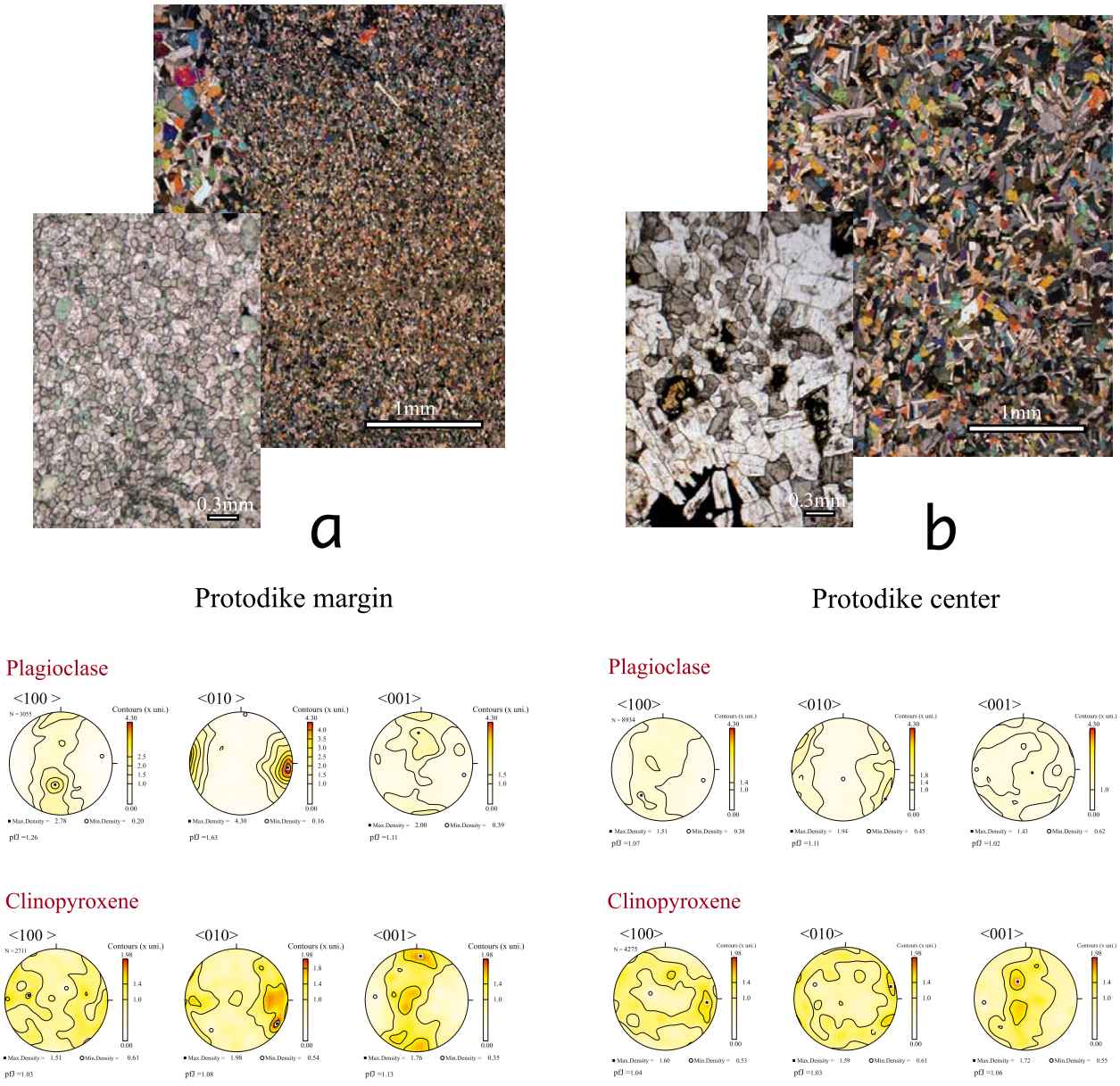

Figure 6. (a) (top) Plane polarized light microphotograph across the margin of a vertical protodike (06OA31) with, superimposed, enlarged and plain light view of the microgranular texture and (below) related crystallographic preferred orientation. (b) (top) Plane polarized light microphotograph of the ophitic protodike center (same sample as Figure 6a), with, superimposed, enlarged and plain light view of the ophitic texture and (bottom) related crystallographic preferred orientation. Crystallographic preferred orientations are Electron BackScattering Diffraction (EBSD) measurements (lower hemisphere, nonpolar data, stereoplot in the structural reference frame with dike margin NS vertical).

ally no more than 10 cm thick. Textures in microgabbro and microgabbronorite lenses compare with the microgranular margins of protodikes, though generally more foliated. They are thought to derive from diabase dikes stopping into the melt lens, and recrystallizing in the water which they introduced [*MacLeod and Rothery*, 1992; *Nicolas et al.*, 2000; *Coogan et al.*, 2003].

[24] In the Aswad area (Figure 2), within the upper granular gabbros about 100 m below the transition to the RZSDC doleritic gabbros, the steep magmatic foliation is locally sharply crosscut by a ~50 m thick sill complex of pegmatitic doleritic

Figure 7. (a) Sill with multiple intrusions of varitextured ophitic gabbros and one protosill, emplaced in the uppermost foliated gabbros (06OA2). (b) Contact between the steeply foliated gabbro (bottom) and the base of the sill (top). Scale bar is 10 cm.

gabbro and protosills (similar to a protodike, but in a sill orientation) (Figure 7).

4. Structural Relationships in Map

[25] The orientation of diabase dikes in the sheeted dike complex is fairly homogeneous (Figure 8), on average 135°E, vertical (Figure 8) which remains unchanged within the RZSDC. The LT hydrothermal veins and the protodikes are oriented 135°E, vertical too and, more loosely, the pegmatitic gabbros and trondjhemite intrusions, which are either close to the sheeted dikes or flat-lying. Foliations in the uppermost foliated gabbros are also, on average, parallel to the sheeted dikes.

[26] Another striking feature of the RZSDC is its limited thickness. Its horizontal extension in the field varies from less than 500 m, which is an upper limit, to less than 200 m in a few places. The average lava flow orientation, 95S25°, may exceed the general dip of the paleohorizontal, because they are located close to the thrust limit of the Sumail massif. We rather rely on the many measurements indicating that in the northern area, between Wadi Abda and north of Ibra road, the crust/mantle boundary is on average oriented 90S15°. An average ESE dip of ~20° seems to be a good estimate for the RZSDC in the considered domain. Bracketing the RZSDC lateral extension between 200 and 500 m, with a 20° dip, its thickness ranges from 70 to 170 m. We retain an average thickness of 100 m which is consistent with previous estimates in Oman [*Rothery*, 1983; *Nicolas and Boudier*, 1991; *MacLeod and Yaouancq*, 2000]. There are, however, minor local variations in thickness, in addition to the major ones described below. A vertical variation of the upper limit of 30 m, over a distance of 100 m has been locally measured in northern Oman.

5. Wadi Gaz Section: Microprobe Analysis

[27] A detailed petrographic and microprobe analysis has been carried on a sampling of Wadi Gaz (Figure 2), in an area covering a complete section from the upper level foliated ophitic gabbros to the sheeted dike complex (Figure 9). The RZSDC extends over ~70 m in thickness, on the eastern slope of the wadi, but continuous exposure is

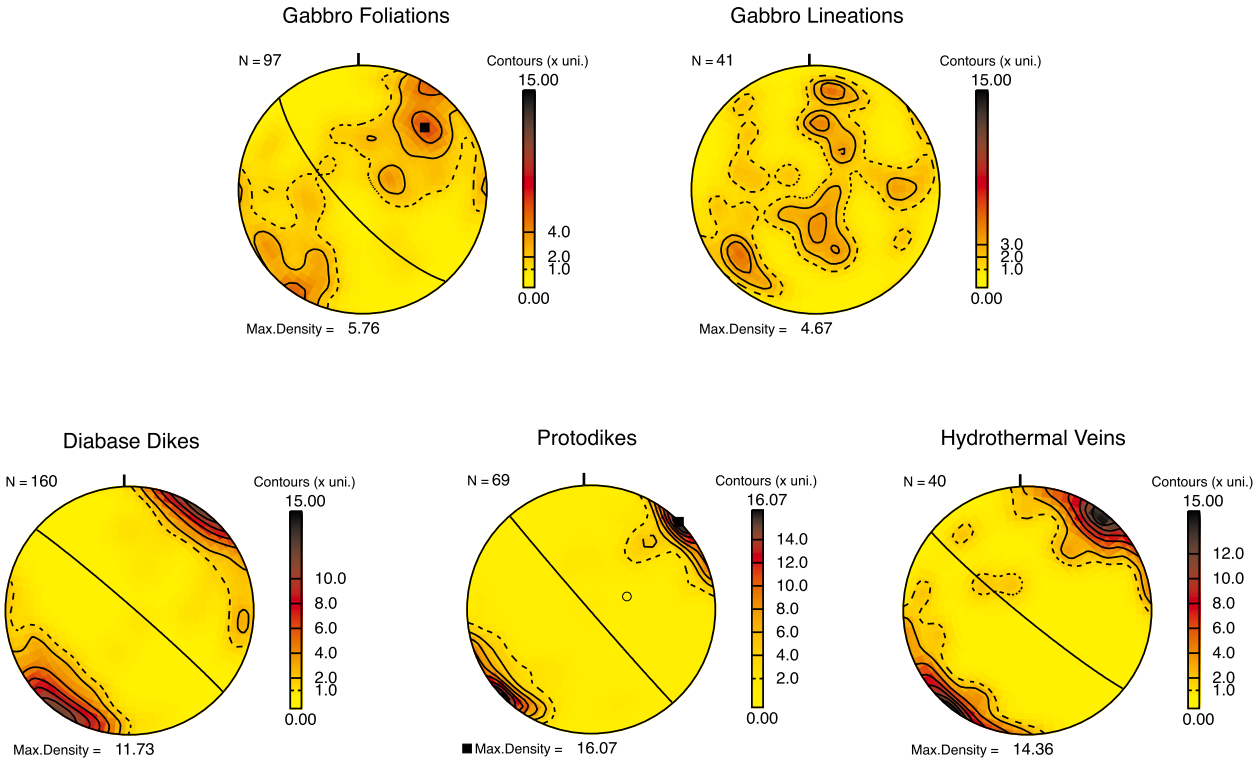

Figure 8. Stereonets of field structures (geographical reference frame, lower hemisphere of projection, nonpolar data). Thirty percent of the measurements come from small areas near Aswad.

Figure 9. Photograph of the Wadi Gaz area sampled for detailed textural and petrographical study. Analyzed samples (Tables 1 and 2) are plotted; see also Figure 2.

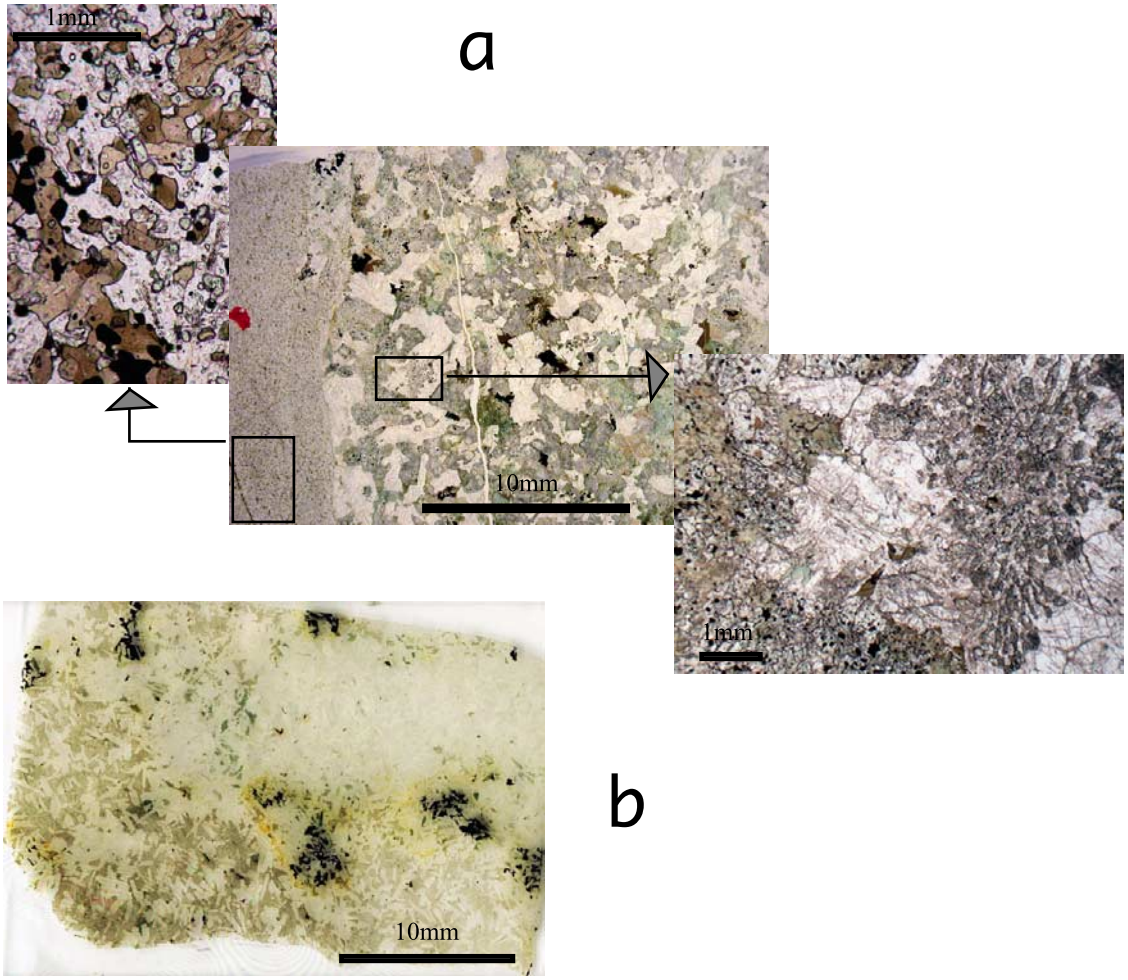

Figure 10. Microphopographs of critical zones studied. (a) Development of granoblastic texture in ophitic gabbro at contact of a microgranular protodike (sample OM06-22). Both ophitic gabbro and protodike contain pargasitic amphibole, specially developed along a microcrack in the protodike. (b) Subophitic domain in contact with intergranular domain at scale of the thin section, in varitextured gabbros (sample OM06-30). The subophitic domain is remarkably fresh and contains poikilitic Ti-rich pargasite associated with poikilitic ilmenite; the intergranular domain is weathered and devoid of oxides.

limited between the wadi bed and the terrace where the upper road circulates (Figure 9). The terrace level is some 10 m below the sheeted dike complex. The base of the RZDSC is well marked by a sharp contact between foliated and isotropic ophitic gabbro. Above this horizon, there is a zone of isotropic gabbros, locally intruded by a sheeted protodike complex, cropping out horizontally and vertically over 10 to 20 m (Figure 5a), a feature which is uncommon and specially well exposed in Wadi Gaz. Protodikes are associated with dioritic intrusions. The center of these dikes is composed of ophitic gabbros, locally displaying a fluidal texture with a crystallographic fabric (Figure 6b), grading outward into microgranular margins (Figure 6a). Microgranular margins are also isolated in the ophitic gabbro matrix, either as slivers or as brecciated blocks. The upper level of the RZSDC is marked by a rapidly increasing abundance of diabase dikes, reaching 50% diabase dikes at the terrace level. Varitextured gabbros, together with trondjhemitic intrusions, are the predominant screens between diabase dikes. The first diabase dikes are metamorphosed in amphibolite facies conditions, containing a brown-green hornblende (Figure 3a), in contrast with the overlying dikes which are in the greenschist facies.

[28] The studied samples are located on Figure 9, their textures are imaged in Figures 3 and 10, they are described in Table 1, and their major elements analyses are presented in Table 2.

Table 1. Description of Analyzed Samples

Sample	Description	Texture	Grain Size	Photograph
OM06-17	foliated granular olivine-gabbro located 900 m beneath the RZSDC, 2 km west of Aswad farm, foliation marked by plagioclase tablets elongation and by alignment of tabular clinopyroxene fresh olivine except oxidation in microcracks, small amount of brown amphibole.	foliated granular	1–2 mm	Figure 3f
OM06-18	foliated equigranular microgabbro lens in OM06-17 gabbro plagioclase, clinopyroxene, no oxides; alteration microveins including mylonite.	microgranular	0.5 mm	
OM06-22	microgranular margin of a protodike including larger (0.1 mm) pargasitic amphiboles and its contact with ophitic gabbro, with pargasitic amphibole.	microgranular (margin)	0.02 mm	Figure 10a
		ophitic (gabbro)	1 mm	
OM06-24 and 25	ophitic gabbro, variable grain size, clinopyroxene interstitial and locally replaced by brown and green hornblende.	ophitic	1–5 mm	Figure 3c
OM06-26	microgabbro, margin of a protodike, rich in oxides (magnetite and ilmenite); except for their rim clinopyroxene phenocrysts have a composition significantly different from clinopyroxene in the matrix.	microgranular	0.1 mm	Figure 5a
OM06-27	ophitic gabbro with HT pargasitic amphibole largely replaced by magnesio-hornblende, both interstitial around clinopyroxene and reactional inside them.	ophitic	3–5 mm	Figure 5a
OM06-28	diorite with plagioclase, interstitial clinopyroxene replaced by magnesio-hornblende rare high-T amphiboles, magnetite, ilmenite.	ophitic	1 mm	Figure 5a
OM06-29	ophitic gabbro with poikilitic clinopyroxene replaced by medium-T magnesiohornblende, totally altered olivine, rare oxides.	ophitic	1 mm	Figure 5a
OM06-30	varitextured ophitic gabbro with 10 mm poikilitic clinopyroxene including plagioclase laths, poikilitic iron oxide, in contact with an intergranular finer-grained domain devoid of iron oxides.	ophitic		Figure 10b
06OA-31b and c	respectively margin and center of a protodike intruding and brecciating ophitic gabbro center and margin of the dike have similar minerals composition.			Figures 6a and 6b
	•margin fine-grained (Figure 6a) with polygonal plagioclase, clinopyroxene with 1% titanium value, totally altered olivine and ~10% interstitial iron oxides.	microgranular	0.1 mm	
	•center ophitic gabbro with prismatic pl and granular clinopyroxene evolving locally in clots of polygonal grains, oxidized olivine.	ophitic	1 mm	

Table 1. (continued)

Sample	Description	Texture	Grain Size	Photograph
06OA-2b	coarse-grained "dry" ophitic gabbro, located at contact with a foliated ophitic gabbro, with plagioclase laths randomly oriented, locally included in 5 to 10 mm sized poikilitic clinopyroxene. hydrous alteration limited to fibrous rims of chlorite and actinolite surrounding olivine interstitial amphiboles (<1%) zoned from brown to blue-green.	coarse ophitic	3–5 mm	Figure 3d
06OA-20a	varitextured ophitic gabbro, pl (~1 mm) zoned and altered, interstitial clinopyroxene (5 to 10 mm), grading into brown, then green amphibole.	ophitic	1 mm 5–10 mm	Figure 3b

[29] On the basis of plagioclase-clinopyroxene compositions, most rocks are highly primitive, with plagioclase, 86% An and clinopyroxene, Mg# 86 (Figure 11). They grade into moderately differentiated gabbroic rocks. The most differentiated rock is dioritic with plagioclase 43% An and clinopyroxene, Mg# 73. No orthopyroxene has been observed in the samples analyzed. The composition of amphiboles is shown in Figure 12, where the estimated thermometry is derived from *Koepke et al.* [2005a], on the basis of reliability of the TiO_2-in-amphibole thermometry, and coexisting amphibole-plagioclase thermometer of *Holland and Blundy* [1994], applied to oceanic gabbros (see detail in Figure 12a). Thus the amphibole compositions constrain the crystallization path of these gabbros. One typical protodike microgranular margin (OM06-22) (see Figure 10a) contains a pargasitic amphibole grown at very high temperature (~1000°C). All sampled gabbros contain, as interstitial or overgrowth phases, pargasites formed at >900°C, down to edenites and magnesiohornblendes, formed at 800–700°C. TiO_2 content of amphiboles is highly variable. We notice that amphiboles with high TiO_2 content (2.55 to 5.07) are high-T pargasitic amphibole that coexist with ilmenite (see Figure 10b), as outlined in the composition of oceanic gabbros [*Koepke et al.*, 2005a]. We notice the wide range in values of TiO_2 (0 to 5% for whole rock) coupled with variable An content in plagioclase that also characterize the varitextured gabbro and dike root zone in the best documented gabbro section of Wadi Abyad in Oman [*MacLeod and Yaouancq*, 2000]. The pargasitic amphiboles in the present study are also rich in fluor (Figure 12b) and, by comparison with compilation of oceanic gabbros by *Coogan et al.* [2001], pargasites from Wadi Gaz area exhibit high chlorine content (1000–2000 ppm), in the same order as amphiboles from the Oman gabbro section compiled by *Coogan* [2003].

6. Discussion

6.1. Structure of the RZSDC in the Mapped Area

[30] A remarkable feature of RZSDC is the common, dominant orientation of all structures parallel to diabase dikes in the sheeted complex (Figure 8): LT hydrothermal veins, tonalite-trondjhemite intrusions, diabase protodikes and foliated gabbros below the RZSDC. As the sheeted dike complex is generally assumed to be parallel to the ridge symmetry plane, most structures in the RZSDC and below should be parallel to the ridge symmetry plane, which also controls the shape of the magma chamber [*Nicolas et al.*, 1988; *Chenevez et al.*, 1998].

[31] This simple RZSDC model is locally modified in different ways, some of which being illustrated in the studied area (Figure 2). West of the Aswad farm, RZSDC formations constitute a sill, 10 m thick, which transects steeply dipping foliated gabbros from the gabbro unit (Figure 7). This may relate to lateral or downward migration of the melt lens position with time. Near the Luzugh oasis (Sumail massif), the RZSDC overlies a flat-lying foliated ophitic gabbros. This is possibly due to rapid lateral migration or subsidence of the melt lens. Subsidence of melt lens has been documented at the East Pacific Rise

Table 2. Minerals Composition

Samples	Lithology	Phase	SiO_2	TiO_2	Al_2O_3	Cr_2O_3	FeO	MnO	NiO	MgO	CaO	Na_2O	K_2O	F	Cl	Total	XMg	Xan
OM06-17	ol-gabbro	ol	38.69	0.02	0.02	0.01	21.97	0.36	0.09	39.70	0.11	0.01	0.01			100.99	76.31	
OM06-17	ol-gabbro	cpx	52.61	0.50	2.26	0.15	6.31	0.20		16.66	21.15	0.28	0.00			100.11	82.48	
OM06-17	ol-gabbro	pl core	48.87	0.04	32.16	0.02	0.48	0.01		0.04	15.96	2.69	0.03			100.29		76.62
OM06-17	ol-gabbro	pl rim	50.06	0.07	31.11	0.01	0.50	0.01		0.07	14.66	3.39	0.07			99.96		70.51
OM06-18	mocrogabbro	cpx	52.14	0.66	2.70	0.16	6.57	0.15		16.18	21.36	0.32	0.00			100.24	81.44	
OM06-18	microgabbro	pl	49.33	0.05	31.89	0.00	0.53	0.02		0.04	15.68	2.92	0.03			100.50		74.78
OM06-22	dike	pl relict	45.42	0.02	34.09		0.49	0.06		0.00	18.46	1.21	0.03			99.79		89.42
OM06-22	dike	pl	56.76	0.04	27.29		0.49	0.01		0.02	9.37	6.37	0.25			100.60		44.83
OM06-22	dike	mt	0.09	5.54	1.29		87.69	0.05		0.00	0.14	0.05	0.00			94.86	0.00	
OM06-22	dike	il	0.08	49.68	0.01	0.02	49.35	2.48		0.05	0.27	0.00	0.00			101.95		
OM06-22	dike	cpx	52.91	0.20	0.81	0.04	9.04	0.29		15.10	22.12	0.31	0.01			100.83	74.86	
OM06-22	dike	am	43.28	3.31	9.49	0.02	13.94	0.19	0.02	13.32	11.36	2.31	0.55	0.07	0.26	98.11	63.01	
OM06-22	granoblastic in gabbro	cpx	51.76	0.59	2.42	0.40	7.85	0.22		15.01	22.12	0.39	0.00			100.76	77.32	
OM06-22	granoblastic in gabbro	am	43.06	2.06	11.06	0.33	12.15	0.17		14.17	11.64	2.33	0.71			97.68	67.52	
OM06-22	granoblastic in gabbro	pl	46.65	0.02	33.79		0.41	0.01		0.00	17.66	1.74	0.04			100.34		84.86
OM06-22	gabbro	cpx	51.67	0.43	2.93	0.46	5.79	0.18		16.41	22.41	0.29	0.01			100.56	83.48	
OM06-22	gabbro	cpx rim	49.70	0.56	2.15	0.66	10.91	0.25		15.12	21.03	0.36	0.01			100.75	71.19	
OM06-22	gabbro	pl	46.41	0.02	33.99		0.44	0.01		0.00	17.70	1.68	0.05			100.30		85.37
OM06-22	gabbro	am	41.95	3.67	10.33	0.09	12.99	0.17	0.03	13.67	11.31	2.80	0.22	0.05	0.15	97.44	65.25	
OM06-22	gabbro	mt	0.07	8.71	1.61	0.81	82.09	0.55		0.21	0.01	0.01	0.01			94.06		
OM06-24	microgabbro	cpx	51.20	0.60	2.32	0.11	6.75	0.19		16.78	20.80	0.31	0.00			99.07	81.58	
OM06-24	microgabbro	am	51.65	0.78	3.06	0.01	14.22	0.26	0.03	16.13	10.43	0.94	0.17	0.05	0.09	97.83	66.91	
OM06-24	microgabbro	pl	50.78	0.05	29.77		0.63	0.04		0.06	13.50	4.07	0.05			98.95		64.71
OM06-25	microgabbro	am	51.27	0.93	4.77	0.40	9.25	0.14	0.02	18.16	11.57	1.23	0.13	0.01	0.10	97.99	77.78	
OM06-25	microgabbro	am	46.48	0.52	9.98	0.02	9.60	0.15	0.03	16.90	11.68	2.21	0.31	0.01	0.13	98.03	75.83	
OM06-25	microgabbro	cpx	51.69	0.76	2.71	0.34	6.64	0.17		16.43	21.26	0.36	0.01			100.36	81.52	
OM06-25	microgabbro	pl	48.55	0.04	32.34		0.31	0.00		0.01	16.06	2.66	0.03			100.01		76.92
OM06-26	microgabbro	il	0.05	50.09	0.01	0.11	44.68	4.99		0.05	0.27	0.01	0.00			100.26		
OM06-26	microgabbro	mt	0.10	9.80	3.65	0.53	77.38	0.48		0.04	0.13	0.01	0.00			92.12		
OM06-26	microgabbro	pl	53.55	0.07	29.14	0.01	0.58	0.01		0.05	12.19	4.87	0.05			100.52		58.04
OM06-26	microgabbro	pl relict	46.32	0.02	33.93		0.49	0.01		0.01	17.86	1.56	0.02			100.20		86.38
OM06-26	microgabbro	pl matrix	52.81	0.07	29.28		0.61	0.02		0.07	12.25	4.80	0.06			99.96		58.49
OM06-26	microgabbro	cpx matrix	50.95	0.96	2.49	0.03	9.29	0.27		14.78	20.86	0.38	0.01			100.01	73.93	
OM06-26	microgabbro	cpx relict	51.76	0.39	3.60	0.95	4.62	0.13		16.58	22.14	0.24	0.01			100.42	86.49	
OM06-26	microgabbro	cpx rim	51.17	0.85	2.57	0.08	9.03	0.26		14.97	20.86	0.37	0.01			100.17	74.73	
OM06-27	gabbro	am core	45.44	2.42	7.89	0.02	15.50	0.22	0.04	13.13	10.78	2.29	0.21	0.18	0.23	98.35	60.16	
OM06-27	gabbro	am rim	51.27	0.53	3.41	0.00	14.48	0.23	0.01	15.69	11.10	1.07	0.09	0.05	0.16	98.09	65.89	
OM06-27	gabbro	am interst	41.27	5.07	11.08	0.03	14.93	0.23		11.45	11.06	2.98	0.08			98.19	57.75	
OM06-27	gabbro	cpx	52.64	0.27	0.71	0.00	9.65	0.35		14.41	21.88	0.24	0.00			100.15	72.69	
OM06-27	gabbro	mt	0.07	9.97	1.46	0.11	82.00	0.47		0.06	0.00	0.01	0.01			94.16		
OM06-27	gabbro	il	0.00	48.05	0.09	0.02	50.26	1.19		0.15	0.03	0.01	0.01			99.81		
OM06-27	gabbro	pl	55.57	0.06	27.74	0.01	0.54	0.01		0.04	10.22	5.68	0.06			99.94		49.85
OM06-27	gabbro	cpx	52.02	0.69	1.76	0.01	9.72	0.28		15.06	20.50	0.38	0.02			100.42	73.42	

Table 2. (continued)

Samples	Lithology	Phase	SiO_2	TiO_2	Al_2O_3	Cr_2O_3	FeO	MnO	NiO	MgO	CaO	Na_2O	K_2O	F	Cl	Total	XMg	Xan
OM06-28	gabbro	cpx	51.20	1.04	1.99	0.01	9.71	0.28		14.92	20.35	0.45	0.01			99.96	73.26	
OM06-28	gabbro	il	0.01	49.45	0.02	0.00	51.00	1.33		0.17	0.06	0.00	0.00			102.04		
OM06-28	gabbro	mt	5.39	12.05	2.52	0.10	68.89	0.60		1.38	2.48	0.01	0.02			93.44		
OM06-28	gabbro	pl	56.69	0.07	26.27		0.50	0.01		0.04	9.19	6.71	0.07			99.56		43.10
OM06-29	ol-gabbro	ol	38.66	0.03	0.01	0.00	24.06	0.44	0.09	37.83	0.06	0.03	0.02			101.23	73.70	
OM06-29	ol-gabbro	pl	47.48	0.04	33.43		0.50	0.02		0.03	16.64	2.11	0.03			100.29		81.34
OM06-29	ol-gabbro	cpx	51.59	0.39	2.69	0.44	4.36	0.13		17.18	21.54	0.25	0.01			98.59	87.54	
OM06-29	ol-gabbro	am	49.82	0.97	5.32	0.02	11.30	0.16	0.03	16.32	11.59	1.20	0.23	0.01	0.24	97.21	72.02	
OM06-30	sub-ophitic gabbro	am	45.88	2.55	7.54	0.01	14.69	0.32	0.01	13.77	10.35	2.74	0.22	0.54	0.13	98.74	62.56	
OM06-30	sub-ophitic gabbro	am	42.60	3.75	11.62	0.02	12.53	0.21	0.00	13.35	11.67	3.06	0.03	0.40	0.03	99.27	65.52	
OM06-30	sub-ophitic gabbro	mt	0.36	8.98	2.14	0.09	82.21	0.17		0.12	0.01	0.04	0.01			94.13		
OM06-30	sub-ophitic gabbro	cpx	52.42	0.93	2.74	0.14	7.07	0.21		16.31	20.59	0.35	0.01			100.75	80.45	
OM06-30	sub-ophitic gabbro	pl core	53.06	0.07	30.13		0.57	0.02		0.07	12.35	4.59	0.05			100.90		59.78
OM06-30	sub-ophitic gabbro	pl rim	65.54	0.00	22.41	0.00	0.26	0.02	0.00	0.00	2.74	10.26	0.11			101.34		12.84
OM06-30	intergranular	pl relict	65.31	0.00	22.50	0.00	0.03	0.01	0.00	0.02	2.89	10.13	0.18			101.06		13.61
06 OA 31c	protodike center	cpx	50.93	0.87	2.63	0.04	8.74	0.19		14.60	20.25	0.39	0.01		0.02	98.78	74.86	
06 OA 31c	protodike center	pl	53.75	0.08	29.35	0.02	0.52	0.02		0.07	11.67	4.96	0.05		0.01	100.56		56.50
06 OA 31c	protodike center	ol	43.17	0.01	10.99	0.03	7.97	0.07		22.79	2.09	0.41	0.04		0.01	87.67	83.59	
06 OA 31b	protodike margin	cpx	50.95	0.92	2.66	0.06	8.79	0.21		14.78	20.48	0.37	0.01			99.26	74.98	
06 OA 31b	protodike margin	pl	53.18	0.09	29.09	0.02	0.60	0.02		0.09	12.10	4.70	0.05			99.95		58.74
06 OA 2b	dry ophitic gabbro	ol	39.01	0.01	0.03	0.03	19.53	0.34		40.80	0.20	0.01	0.01		0.00	99.97	78.83	
06 OA 2b	dry ophitic gabbro	pl core	48.25	0.04	32.35	0.03	0.48	0.02		0.05	16.06	2.39	0.03		0.01	99.73		78.79
06 OA 2b	dry ophitic gabbro	pl rim	52.41	0.08	29.56	0.03	0.47	0.02		0.07	12.98	4.22	0.06		0.00	99.91		62.95
06 OA 2b	dry ophitic gabbro	cpx	50.94	1.42	3.09	0.08	6.09	0.19		15.40	21.49	0.46	0.01		0.01	99.29	81.85	
06 OA 2b	dry ophitic gabbro	br-am	44.53	3.49	9.02	0.01	10.14	0.18		15.28	10.63	3.22	0.31		0.03	97.16	72.87	
06 OA 2b	dry ophitic gabbro	am	57.54	0.04	0.46	0.01	3.78	0.11		22.37	12.46	0.23	0.00		0.00	97.21	91.35	
06 OA 2b	dry ophitic gabbro	am	43.36	0.47	10.59	0.01	19.63	0.40		8.68	11.58	1.92	0.16		0.06	96.92	44.06	
06 OA 2b	dry ophitic gabbro	am II	47.14	0.44	8.85	0.02	8.19	0.13		17.90	11.32	2.65	0.25		0.10	97.28	79.58	
06 OA 2b	dry ophitic gabbro	chl	29.58	0.02	18.25	0.02	15.12	0.21		22.24	0.08	0.07	0.16		0.01	85.86	72.38	
06 OA 20	ophitic gabbro	br-am	43.92	3.00	10.24	0.04	12.74	0.17		13.61	10.89	2.59	0.41		0.23	97.92	65.57	
06 OA 20	ophitic gabbro	gr-am	47.26	0.61	8.38	0.03	13.44	0.16		14.09	11.30	1.96	0.20		0.19	97.73	65.14	
06 OA 20	gabbro	pl	47.24	0.05	34.25	0.00	0.60	0.01		0.01	16.80	2.23	0.03		0.02	101.32		80.65
06 OA 20	gabbro	pl rim	51.79	0.11	30.85	0.03	0.58	0.03		0.05	12.99	4.11	0.13		0.01	100.80		63.60

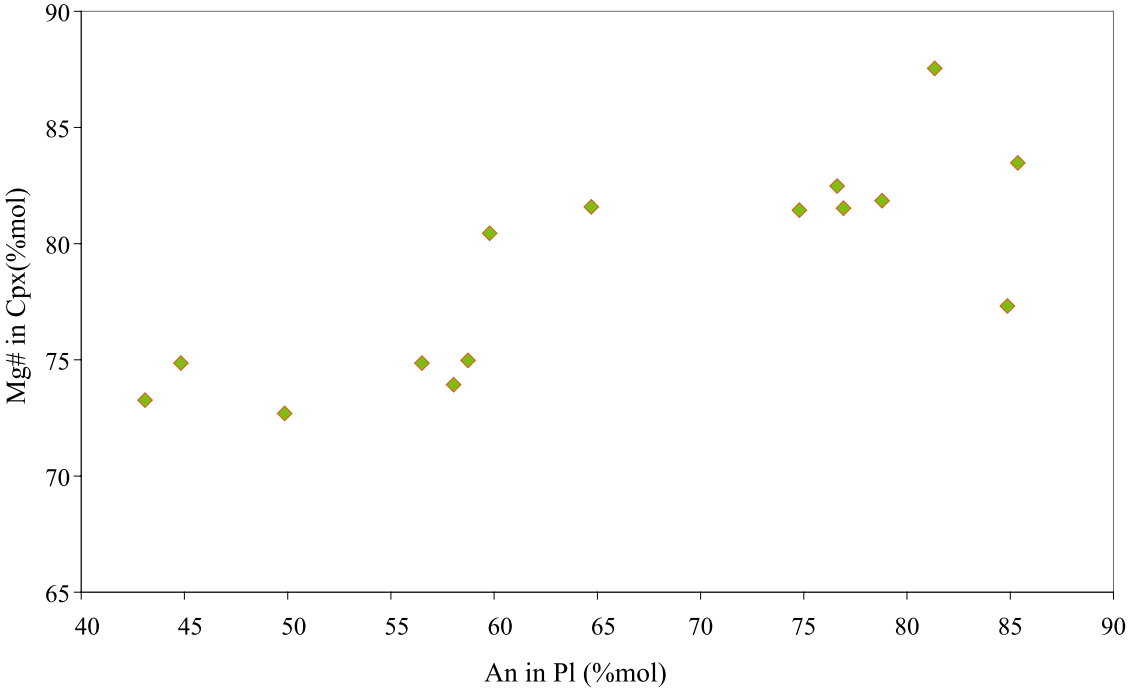

Figure 11. Composition of plagioclases and clinopyroxenes of the Wadi Gaz dike rocks (see analyses in Table 1).

[*Hooft et al.*, 1997; *Lagabrielle and Cormier*, 1999; *Garel et al.*, 2002]. Conversely, a rise of the melt lens would result in an assimilation of its roof, as also envisaged by *Coogan et al.* [2003]. This could explain the local abundance of micro-gabbro-norite lenses locally interlayered within the foliated and layered gabbros.

6.2. Wadi Gaz as a Typical Section Through the RZDSC

[32] We have defined the base of the RZDSC in the Wadi Gaz section (location in Figure 2) as coinciding with both the floor and the roof of a melt lens (cross section in Figure 2). This important boundary has been traced in the field on the western side of the Wadi Gaz (Figure 9). It is where the floor and the roof of the melt lens were squeezed together when the melt lens closed, due to drifting away from the ridge axis. After settling on the floor of the lens, the gabbro mush subsided within the magma chamber and rotated, developing a steep foliation which was frozen when this mush solidified as a gabbro and drifted out of the magma chamber [*Quick and Denlinger*, 1993; *Chenevez et al.*, 1998] (Figure 13a). The uppermost, crude and steep foliation taken as the top of the RZSDC has been developed right at the limit of the melt lens. The roof of the melt lens has crystallized at <1200°C in dry conditions as a coarse and dry ophitic gabbro, representing the base of the RZSDC and locally preserved (Figure 13c). Above, we interpret the RZSDC isotropic ophitic gabbros as related to successive stages of protodike intrusions. The protodikes were injected near the roof of the melt lens where temperature was in the range of 1100°C–1000°C (Figure 13c). The center of the dikes crystallizes as isotropic ophitic gabbros with microgranular margins resulting from a rapid cooling at the contact with the hot and hydrated ophitic gabbros. Protodikes would be split by subsequent dike-in-dike intrusions in a medium also submitted to hydrous recrystallization and anatexis. As a result, protodikes would be mostly destroyed and, usually, only recalled by slivers or breccias of their microgranular margins within an ophitic gabbro matrix. This is typically seen in Wadi Gaz where, exceptionally, a small sheeted protodike complex has been preserved. A few tens of meters above this complex, the isotropic ophitic gabbros partly recrystallize and melt by hydrous anatexis. Pegmatitic veins in varitextured gabbros and minor trondjhemite intrusions are generated by this anatexis. Finally, we have described at the base of the greenschist facies sheeted dike complex a limited horizon of amphibolite facies diabase dikes. They would represent a thermal boundary layer between the HT RZSDC and the overlying LT sheeted dike complex.

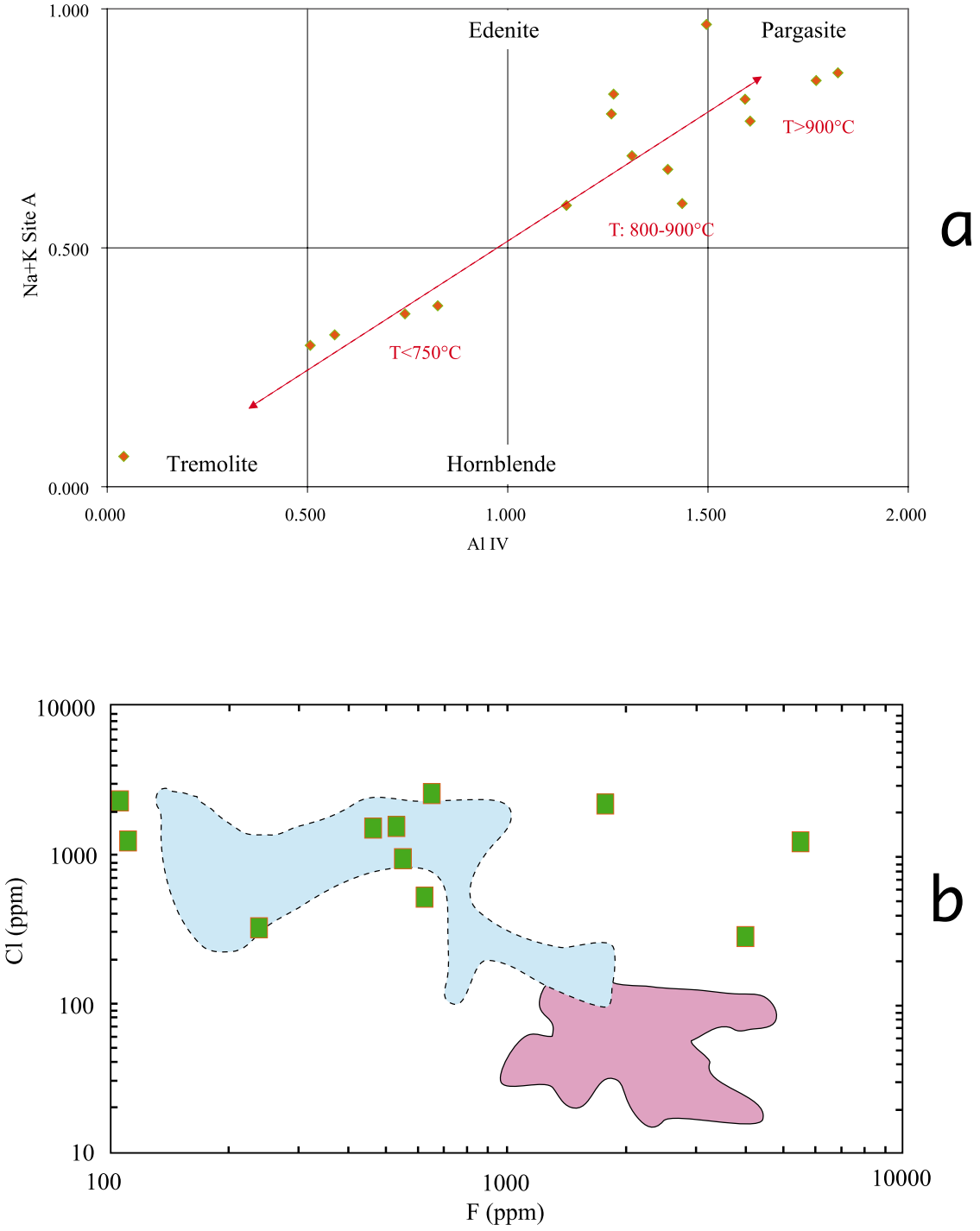

Figure 12. (a) Compositions of amphiboles from the Wadi Gaz dike rocks (see analyses in Table 1). For the estimation of equilibrium temperatures based on coexisting amphibole-plagioclase, we used the thermometer of *Holland and Blundy* [1994]. Moreover, temperatures for amphibole formation were derived by applying the semiquantitative geothermometer of *Ernst and Liou* [1998] based on the Ti content in amphiboles. For this, only those amphiboles were used which coexist with a titanian oxide phase (titanomagnetite or ilmenite). Previous studies in basaltic systems showed the general good agreement between the Ti-in-amphibole and amphibole-plagioclase temperatures [*Koepke et al.*, 2005a]. Moreover, the reliability of the TiO_2-in-amphibole thermometer was confirmed by an experimental study of *Koepke et al.* [2004] where temperatures derived from the TiO_2 content in amphiboles of experimental products correspond well to the temperatures of the experimental runs. (b) F versus Cl in amphiboles from the Wadi Gaz rocks (see analyses in Table 1). Fields shown are from *Coogan et al.* [2001], vein and replacive (dotted line), bleb and interstitial (full line).

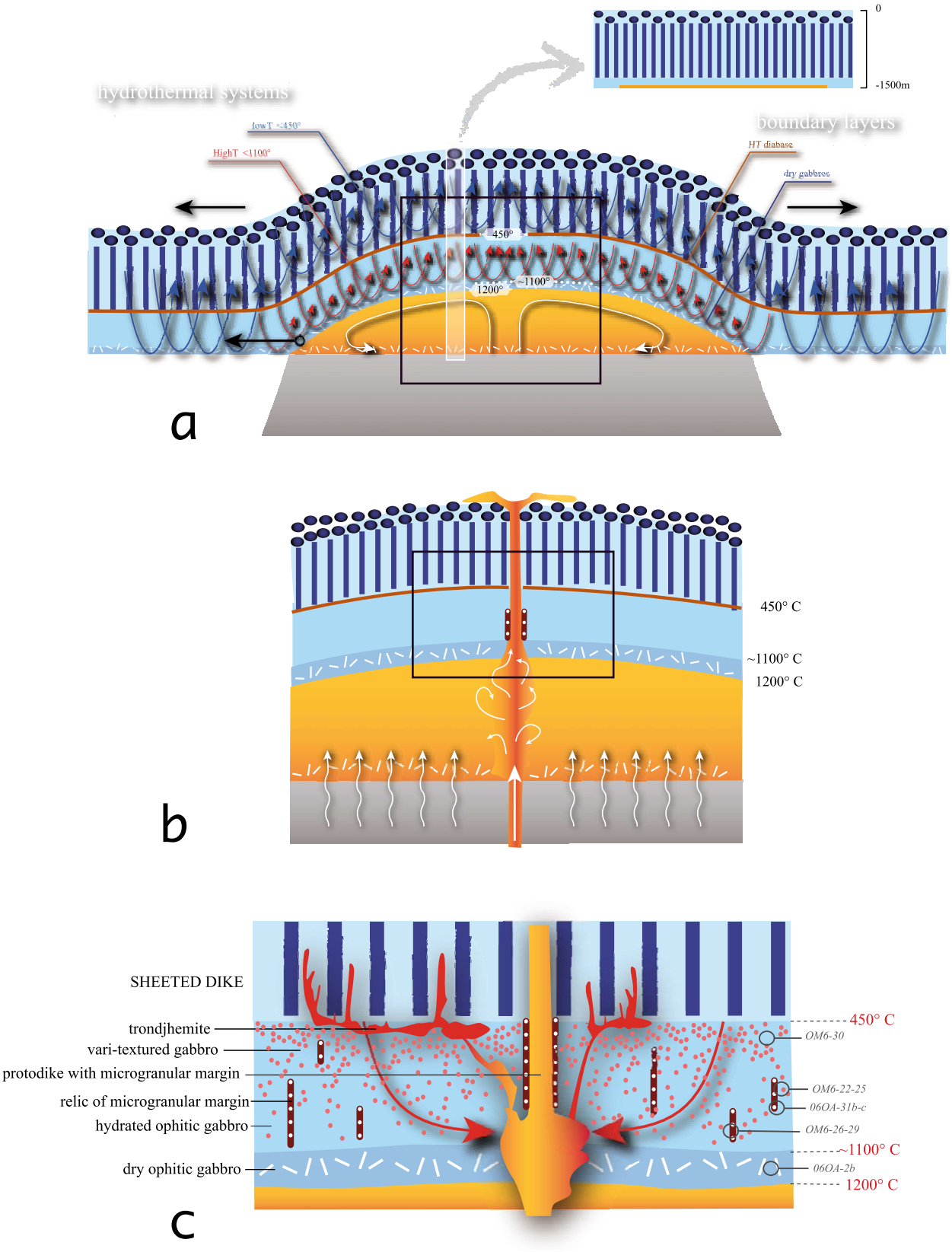
0
-1500m
hydrothermal systems
boundary layers
lowT <450°
HighT <1100°
HT diabase
dry gabbros
450°
1200°
~1100°
a
450° C
~1100° C
1200° C
b
SHEETED DIKE
trondjhemite
vari-textured gabbro
protodike with microgranular margin
relic of microgranular margin
hydrated ophitic gabbro
dry ophitic gabbro
450° C
OM6-30
OM6-22-25
06OA-31b-c
OM6-26-29
~1100° C
06OA-2b
1200° C
c

Figure 13

6.3. Hydrous Anatexis

[33] As already concluded by *Nicolas and Boudier* [1991], field observations convincingly suggest that the varitextured gabbros and their pegmatitic patches grading in pegmatite veins as well as the diorite and trondjhemite bodies are in situ products of hydrous anatexis. This interpretation has been confirmed by the discovery in Oman gabbros of a massive alteration by large fluxes of seawater heated to temperatures up to 1000°C which locally trigger hydrous anatexis [*Nicolas et al.*, 2003; *Bosch et al.*, 2004]. As the same evidence is present in RZSDC, this general interpretation is extended here, noting that seawater ingression should be easier at this shallow level than deeper in the gabbro unit. The interpretation of the observed phase relations as hydrous melting is in agreement with experiments, which have been conducted at the appropriate pressure, temperature, oxygen fugacity (see Figure 14 and Appendix A). On the basis of the mineral analyses reported in Table 2, we can extend the role of water to lower temperatures. Thus, in varitextured gabbros, hydrous reactions responsible for zonation in amphiboles record temperatures dropping from T > 900°C to T < 750°C (Figures 3b and 12a). We have also described within pegmatitic patches, the latest stage of magmatic evolution which were converted into greenschist facies probably by autometamorphism (Figure 4b). Also as a product of a very late stage magmatism, veins, dikelets or small stocks of diorite to trondjhemite can be observed. These felsic compositions can be generated either by advanced differentiation of the hydrous gabbroic mush freezing later to varitextured gabbros or by partial melting of the just frozen gabbro by the introduction of a small amount of seawater at temperatures between 900 and 980°C [*Koepke et al.*, 2004] (Figure 4c). A model-dependent confirmation is provided by *Coogan et al.* [2003]. By balancing the Cl content observed in fresh EPR MORBs with a potential contaminator, the authors conclude that ~20% of hydrothermally altered crust was assimilated and mixed in the melt lens basalt by stopping of altered dikes that can contain high amounts of water due to the presence of hydrated minerals. This also implies that the generation of hydrous magmas within the RZSDC is easily possible, since the addition of small amounts of water at the given shallow pressure may lead to high water activities (see section 6.4 and Appendix A).

6.4. Origin of Water

[34] The question raised here is whether water of mantle origin, carried by the basaltic melt to the melt lens would be sufficient to generate the hydrous reactions recorded in the RZSDC or whether seawater infiltration is necessary. In the experiments reported in Appendix A, under the chosen pressure of 50 MPa, the solubility of water in a primitive MORB melt is 2.2 wt% [*Berndt et al.*, 2002]. Thus, high water activities can be reached easily, with the addition of relative small amounts of water. Even less than 2.2 wt% water is sufficient for reaching water-saturated melts, when the melt fraction is reduced. For instance, only ~1 wt% total water is necessary, for shifting the system of Figure 14 at 1060°C from the dry solidus into a hydrous partly molten regime with ~50% water-saturated melt and 50% anhydrous crystals. Lower water contents are enough to stabilize water-saturated trondjhemitic melts at lower temperatures, where the melt fractions are low (e.g., ~0.1 to 0.4 wt% total water as a function of temperatures and melt fraction). Such low fractions of water can be attained by fractional crystallization of a basaltic melt issued from the

Figure 13. Sketches illustrating, with increasing detail, the internal structure and dynamics of the RZSDC. (a) Convective structure and RZSDC zonation above and away from the melt lens (vertical scale is exaggerated; realistic thickness shown in the close-up). The magmatic convection in the lens (white lines) is separated from the HT hydrothermal convection (red lines) by a dry isotropic ophitic gabbro horizon forming a thermal boundary layer. LT (greenschist facies) hydrothermal convection coincides with the top of the RZSDC, being separated from the underlying HT hydrothermal system by a second thermal boundary layer (amphibolite facies diabase). In the HT hydrothermal regime, hydrous melting of the isotropic gabbros and crystallization generates the varitextured gabbros and trondjhemites. (b) See box in Figure 13a. Intermittent generation of new RZSDC to replace the one drifted off-axis, by cracking of the dry gabbro layer, with injection of new melt through the crack. Dry gabbros crystallize from this new melt which can also be injected as a protodike that extends upsection into a new dike in the sheeted dike complex. (c) See box in Figure 13b. Melt surge through a protodike and minor intrusion at the base of the RZSDC, yielding the crystallization of the isotropic ophitic gabbros presumably in wet conditions, followed by abundant HT hydrous melting in the main body of the RZSDC, generating varitextured and pegmatitic gabbros, diorite, and trondjhemite.

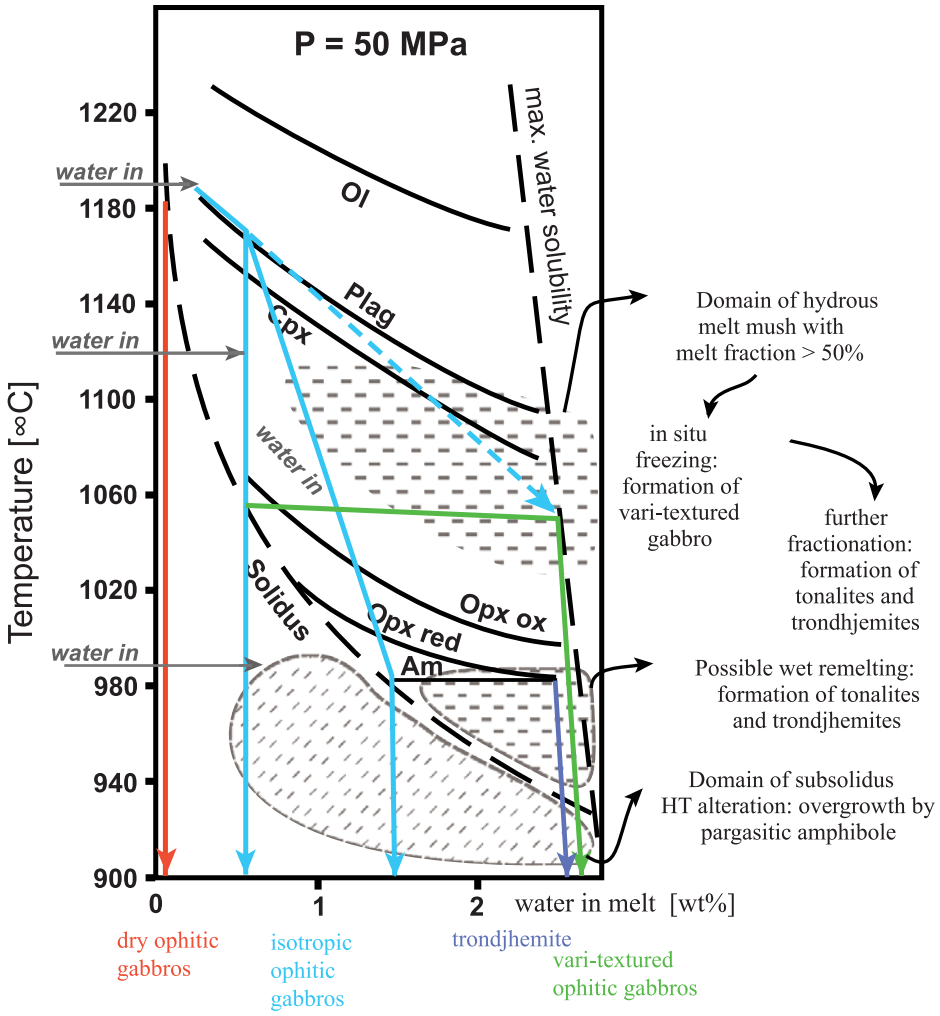

Figure 14. Phase relations in a hydrous primitive tholeiitic system at 50 MPa in the RZSDC. The solid black lines correspond to the phase boundaries of olivine (Ol), plagioclase (Plag), clinopyroxene (Cpx), orthopyroxene (Opx) under oxidizing (ox) and reducing (red) redox conditions, and amphibole (Am). See text for further details on the cooling paths and outlined fields; see Appendix A for background data of the phase diagram.

mantle where the initial water fraction is ~0.05%. The validity of the concept of fractional crystallization when dealing with a melt lens functioning in steady state conditions could be questioned. Thus, it seems quite possible that a minor fraction of deep water can be introduced within the RZSDC. However, on the basis of oxygen isotopes [*Gregory and Taylor*, 1981; *Bosch et al.*, 2004] volumes of water much larger than a few percent are probably available. They indicate that the amount water which permeated Oman gabbros at HT was of the order of magnitude of the mass of these gabbros.

[35] Most gabbros in RZSDC contain pargasitic amphiboles as interstitial or overgrowth phases. According to *Coogan et al.* [2001], the generally high chlorine content of pargasitic amphiboles, like the ones here, indicate that they crystallized in presence of seawater derived fluids. However, the Wadi Gaz pargasitic amphiboles have also a high TiO_2 content, correlated with a high fluor content (Figures 12a and 12b). High values of these two elements are considered as the signature of magmatic amphiboles [*MacLeod and Yaouancq*, 2000; *Coogan et al.*, 2001]. At this stage, we discern that the question of magmatic versus hydrothermal origin of pargasitic amphiboles cannot be settled by our data. *Koepke et al.* [2005a] point out in oceanic gabbros, a correlation of TiO_2 enrichment in pargasitic amphiboles and their association with ilmenite. This correlation is also observed here and

we refer to the discussion of this topic in their paper.

6.5. A General Model for the RZSDC Formation

[36] The model developed now integrates the observations reported above in Wadi Gaz. It applies to RZSDC generation in the situation where, as deduced from the continuity of structures over a transversal distance in map of 15 km (Figure 2), the spreading has been steady state and, expectedly, the melt lens, fairly stable over a period of ~300,000 years (assuming a half spreading rate of 5 cm/a). Subsequently, we will examine the situation of RZSDC in the environment of ridge segmentation.

[37] A dry basaltic melt crystallizes at the roof of the melt lens as a thin layer of coarse-grained and little altered ophitic gabbro. This layer is a thin thermal boundary layer between the magma convection in the melt lens, at ~1200°C, and the HT (>450°C) hydrothermal convection above. Hydrothermal convection rapidly decreases the temperature upsection but the temperature is as high as ~1100°C at the contact with the dry ophitic gabbros (Figures 13a and 14). The complex RZSDC lithology demonstrates the presence of HT fluids inducing both wet anatexis and metamorphic hydrous reactions. The mechanism by which seawater penetrates the RZSDC at high temperatures seems to be simpler here than in the case of the ubiquitous HT hydrothermal alteration of the gabbro unit located below the RZSDC [*Nicolas et al.*, 2003; *Nicolas and Mainprice*, 2005]. In contrast with the latter situation, where HT fluids have to progress several kilometers below the limit of the elastic lithosphere (~600°C), this limit is located here at the base of the sheeted dike complex, ~100 m above the RZSDC. Consequently, seawater can be introduced through tensile stress driven cracks in the elastic lithosphere.

[38] Constrained by experimental studies on the dependence of gabbro stability on water content, at 50 MPa (the approximate pressure conditions of the RZSDC at the ridge axis) (see Appendix A), the phase diagram of Figure 14 describes the formation sequence of igneous rocks in the RZSDC. The dry gabbros plated at the roof of the melt lens crystallized around 1180°C at the dry solidus. From there, they follow the red path in Figure 14. This path is also possible for the overlying isotropic ophitic gabbros which would then also be within the thermal boundary layer. However, because they display distinct textures (Figure 3), these isotropic ophitic gabbros are thought to be related to the HT hydrothermal system above the thermal boundary layer. These isotropic ophitic gabbros would crystallize from a hydrous melt which, at >1100°C following the blue path in Figure 14. This melt would result from the reaction of <1% of hydrothermal fluids with either the dry and solid gabbros from the roof of the melt lens or a dry melt injected through the protodikes.

[39] Protodikes are expected to play a major role in generating the isotropic gabbros (Figures 13b and 13c). Let us assume that a basaltic melt surge cracks the dry gabbro layer from the melt lens roof and progresses to the surface through the sheeted dike complex. It will cross the RZSDC as a melt conduit with possibly lateral injections into the surrounding medium. Just above the roof thermal boundary layer, this will be an active protodike with a microgranular margin. This margin will subsequently remain little changed, possibly because it is fine-grained and not porous. After the melt surge, the interior of the conduit crystallizes in the presence of a hydrous fluid at >1100°C, forming isotropic doleritic gabbro. Related to drifting off-axis, the RZSDC is continuously created by similar melt conduit injections and crystallizations.

[40] Above this lower horizon, more seawater-derived fluids injected at temperatures between 1100°C–1050°C locally induce, in the isotropic ophitic gabbros, hydrous anatexis resulting in crystallization of HT vary-textured and pegmatitic gabbros (Figure 14). The 1100–1050°C temperature interval for intrusion of hydrous fluids is controlled by the fact that below a melt fraction of 50%, it seems difficult, in melting varitextured gabbros, to separate and inject pegmatitic dikes without preserving restitic assemblage. Moreover no restitic assemblages are identified in the field. Due to continuous hydrous intrusion and melting, diorites and trondjhemites can be generated either by advanced closed-system differentiation of the hydrous magma or by subsequent hydrous partial melting events at lower temperatures 900 to 950°C (Figure 14) [*Koepke et al.*, 2005b]. Below this temperature, further hydrothermal alteration takes place only by solid-state metamorphic reactions.

[41] A second thermal boundary layer, located at the base of the sheeted dike complex, exists between the HT and LT hydrothermal convection systems. In Oman, it can be traced by the presence in diabase dikes of HT (amphibolite facies) alter-

ation (Figure 3a), without significant evidence of the LT (greenschist facies) ubiquitous alteration which is present in the overlying dikes.

[42] With seafloor spreading, RZSDC lithologies drift off-axis, probably without any significant change until they pass over the lateral limit of the lens. Beyond this limit, because of the related sharp drop in temperature, the dry doleritic gabbros are submitted, for a short time, to HT hydrothermal alteration. A few outcrops have nearly escaped this alteration and could still represent the roof horizon of the melt lens (Figure 3d).

[43] If melt pulses renew the gabbro boundary layer through melt fractures (Figure 13b) then each diabase dike in the sheeted dike complex is connected to one protodike in the RZSDC. However, protodikes are not that common in the RZSDC. We, therefore infer that the protodikes are massively destroyed, mainly by dike-in-dike intrusions at melting temperatures, and/or by hydrous remelting. As illustrated by Figure 13c, this hypothesis is supported by the observation of protodikes being commonly dismembered, with dispersal of microgranular margins, mainly as breccias and aligned lenses in an ophitic gabbro matrix (Figure 5). The margins of the protodikes have a tighter texture and are more resistant to assimilation than the ophitic center of protodikes. The margins are the only relicts of a former sheeted protodike complex.

6.6. RZSDC in Domains Affected by Ridge Segmentation

[44] We have selected a domain located away from ridge segment limits and related propagating rifts, where ridge segmentation has induced major ridge-related tectonic deformations and magmatic intrusions within the RZSDC. Using the presence of symptomatic gabbronorite and diorite-trondjhemite bodies, restricted to these domains, it is inferred that nearly half the lithosphere has been generated in the Oman ophiolite under the influence of ridge segmentation.

[45] In RZSDC from ridge segmentation domains, the large magmatic intrusions can induce by reheating a local contact metamorphism, as described around a gabbronorite intrusion in Troodos [*Gillis and Roberts*, 1999; *Gillis and Coogan*, 2002]. Conversely, in our RZSDC where no such intrusions are observed, reheating to HT conditions can be induced only along the protodikes emplaced in the hotter, basal part of the RZSDC (Figure 10a). Such contact metamorphism has been observed, but restricted to a centimeter scale. This is not surprising considering that, with a ~7°C/m thermal gradient, the RZSDC experiences an incredibly sharp cooling.

6.7. Comparison of RZSDC in Oman and in the IODP Hole 1256D

[46] The first results of the successful drilling through the floor of a RZSDC in the East Pacific Rise [*Wilson et al.*, 2006] show many similarities with what is observed in Oman (Figure 15) and in other ophiolites, such as Troodos [*Gillis and Roberts*, 1999]. Two features seem particularly characteristic. The IODP and Oman RZSDC have a comparable ~100 m thickness if, according to *Wilson et al.* [2006], the top gabbros from the gabbro unit are represented by the last meters of the core. Most textures observed in the Hole 1256D also match those in Oman, as illustrated by the comparison of ophitic gabbros (Figures 15a and 15b; see also for Troodos ophiolite [*Gillis and Coogan*, 2002]). Interestingly, the "completely recrystallized granoblastic" texture of Figure 4B of *Wilson et al.* [2006] observed in the lower sheeted dikes and equilibrated at ~650°C, matches, in terms of texture and position, our lowermost HT diabase dikes, which corresponds to the thermal boundary layer between the HT and LT hydrothermal systems (Figures 15c and 15d). However, in the IODP leg, the granoblastic dikes section, stratigraphically above the gabbros, is 60 m thick [*Wilson et al.*, 2006], which is somewhat thicker than the HT alteration front at the base of Oman sheeted dike complex.

[47] On the basis of the observation of prograde mineral reactions in the granoblastic dikes, the "granoblastic" textures are ascribed by *Teagle et al.* [2006] and *Wilson et al.* [2006] to "contact metamorphism by underlying gabbro intrusions." This agrees with the Troodos ophiolite study [*Gillis and Roberts*, 1999], where a large metamorphic aureole has been observed in sheeted dikes at the margins of a gabbronorite intrusion. In the part of the Oman RZSDC devoid of late magmatic intrusions, there is no evidence of any reheating, except on a centimeter scale at the margin of a dike. We suggest that Troodos ophiolite, as well as the IODP hole in the Cocos oceanic lithosphere were both accreted in a domain of ridge segmentation and not

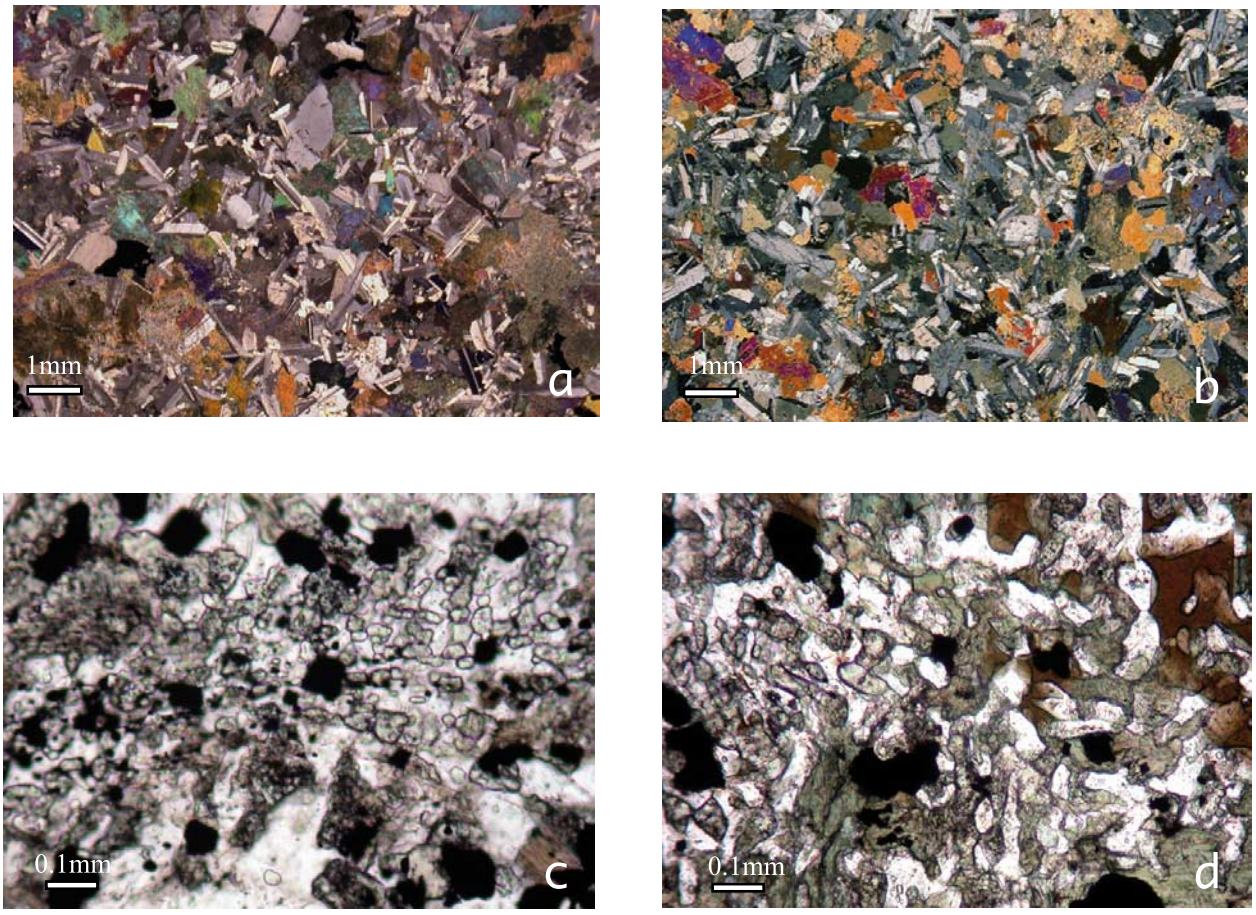

Figure 15. Comparison of textures in the Oman and IODP Hole 1256D RZSDC. The top micrographs show isotropic hydrated ophitic gabbro from (a) IODP sample 1256D216R1 and (b) site 90OF15 in Oman. The bottom micrographs show HT diabase with polygonized Cpx crystals and development of brown hornblende from (c) IODP sample 1256D194R1 and (d) site 03OA62 in Oman.

in a domain of steady state seafloor spreading as in the area selected in Oman for this study.

7. Conclusion

[48] The object of this paper was to revisit RZSDC zones in the Oman ophiolites, at a time when this critical zone has been drilled in the ocean for the first time with IODP Hole 1256D. We wish to insist on the exceptional interest of the RZSDC, as a key to understand crustal accretion at fast spreading centers. A large part of the lower crust is issued from a tiny melt lens, only ~2 km in cross section and ~30 m thick. On top of it, the slightly thicker RZSDC (~100 m) is a horizon in which the temperature drops ~800°C, from 1200°C in the melt lens to 450–400°C at the base of the sheeted dike complex. This represents the most energetic system in dynamic equilibrium at the surface of the Planet that results in the complex and varied lithology described herein. A brief comparison between the RZSDC in Oman and the first descriptions from IODP Hole 1256D suggests that the present study could help to constrain the three-dimensional context of this most important section drilled in the ocean.

Appendix A: Experimental Constraints on the Phase Relations in a Hydrous Primitive Tholeiitic System for a Pressure of 50 MPa (Figure 14)

[49] The rationale behind the understanding of the different magmatic lithologies in the RZSDC is based on the knowledge of the phase relations in a hydrous primitive to moderately evolved tholeiitic system for the pressure conditions of the RZSDC, which is assumed to be 50 MPa (corresponding to

a thickness of ~1 km for the crustal lid, plus 2–3 km water column). The role of water and oxygen fugacity on the phase equilibria and differentiation in tholeiitic, MORB-type systems at shallow pressures has been studied in recent experiments by *Feig et al.* [2006] and S. T. Feig et al. (Effect of oxygen fugacity on phase equilibria in a hydrous tholeiitic basalt, submitted to *Contributions to Mineralogy and Petrology*, 2008). They studied the pressure dependence (100, 200, and 500 MPa) and the role of oxygen fugacity (corresponding to QFM-3 to QFM+4, with QFM = quartz-fayalite-magnetite oxygen buffer) of a primitive tholeiitic system (Mg# = 73.5, with Mg# = molar 100 · MgO/(MgO + FeO)). The phase diagram of Figure 10 is based on an extrapolation of the phase relations to 50 MPa for an oxygen fugacity corresponding to ~QFM-1 at dry conditions and QFM+2 at water-saturated conditions. *Feig et al.* [2006] showed that typical thermodynamic models for predicting magmatic evolution trends like ''MELTS'' [*Ghiorso and Sack*, 1995] and ''Comagmat'' [*Ariskin*, 1999] fail to predict the experimental phase relations under hydrous conditions at shallow pressure. Therefore, the extrapolation of their results to 50 MPa seems the only possible way to estimate reliable evolution trends of a primitive hydrous tholeiitic system at the magmatic conditions prevailing in the RZSDC.

A1. Relation Between Water and Oxygen Fugacity

[50] In a hydrogen-buffered system, as it is the case for such experiments, the prevailing oxygen fugacity strongly depends on the water activity of the system. For the dry and water-poor conditions of Figure 10, we choose an oxygen fugacity corresponding to QFM-1 to QFM which is in accord with recent studies estimating the redox conditions of natural MORB [e.g., *Bezos and Humler*, 2005]. A further hydration of the system consequently leads to more oxidizing conditions resulting in an oxygen fugacity ~QFM+2 for a water activity of 1 (water-saturation). The quantitative treatment of the relation between water activity and redox conditions (and oxidation state of iron) is given by *Botcharnikov et al.* [2005]. The water-saturation curve included in the phase diagrams is obtained from the water solubility in a primitive MORB of *Berndt et al.* [2002] and from the temperature and pressure dependence on water solubility of *Holtz et al.* [1995].

A2. Stability of Oxides

[51] Chrome spinel, which is always stable in the experiments at near liquidus conditions, is not included into the phase diagram of Figure 10. Fe-Ti oxides were not stable under the given redox conditions in the experiments of *Feig et al.* [2006; submitted manuscript, 2008]; they are stable only at more oxidizing conditions. However, since the experimental system is primitive (FeO^{tot} content of 6.5 wt%), it is expected that in a more evolved system, Fe-Ti oxides would be stable at lower temperatures, at least at the more oxidizing conditions in the hydrated regime. The amphibole, which is stable at low temperatures typically shows a pargasite composition.

A3. Effect of Water

[52] The main effect of water on the phase relations in the given system is to displace the stability curves of the minerals at lower temperatures. Under the low pressure of 50 MPa, water is not changing the order of crystallization, in contrast to what is observed at higher pressure. The well-known depression of plagioclase stability (plagioclase crystallizing after clinopyroxene) with increasing water content was observed in the experiments of *Feig et al.* [2006] only at pressures $\geq$200 MPa. Moreover, water content also affects the mineral compositions. According to *Feig et al.* [2006], the An content of plagioclase may increase about 10 to 15 mol% when increasing the water activity from 0 to 1 at a given temperature, while the Mg# of olivine and clinopyroxene is shifted to higher values (maximum of 5 to 10) due to the increased oxygen fugacity with water. Thus, the overall effect of water is to stabilize crystal mushes with moderate or high melt fractions to lower temperatures, and thereby shifting the An content of plagioclase and the Mg# of clinopyroxene and olivine to higher values. Amphibole, the only hydrated phase in the system, is only stable at very low temperatures. Thus, it should be emphasized that the absence of amphibole in crystallized gabbro does not necessarily mean that the conditions in the magma chamber were ''dry.''

A4. Effect of Composition

[53] The system used for our phase diagram is fairly mafic in composition, thus corresponding to one end-member of the range of melts leaving the magma chamber. This has several consequences: (1) liquidus temperatures (and the saturation temperatures of the individual minerals) are high;

(2) olivine is stable down to the lowest temperatures; (3) the stability of orthopyroxene is restricted to the lowest temperatures while olivine is still present; (4) the iron content in the low-temperatures melts are too low for saturating Fe-Ti oxides at the applied redox condition. By using a slightly more evolved system, e.g., a normal MORB with a Mg# of 67 [*Berndt et al.*, 2005], the liquidus temperature of the system (and the saturation temperatures of the individual minerals) are slightly lower (e.g., 1220°C for the dry solidus), but the phase topology is the same and the other points mentioned above are still valid. Only when the system evolves further (e.g., Mg# < 60), notable changes in the phase relations are expected. These can be extrapolated from the experiments in hydrous MORB by *Berndt et al.* [2005], who studied both primitive and evolved MORB: (1) liquidus temperature (and the saturation temperatures of the individual minerals) are lower (e.g., ≤1200°C for the dry solidus); (2) olivine may become unstable; (3) the stability of orthopyroxene is enhanced to higher temperatures; (4) Fe-Ti oxides become stable in the lower temperature part of the diagram (but still strongly depending on the prevailing redox condition).

A5. Stability of Orthopyroxene in a Primitive System

[54] According to *Feig et al.* [2006], at a given pressure, the orthopyroxene stability is increased by oxidizing redox conditions, and decreased with increasing water activities. Therefore, two orthopyroxene saturation curves are displayed in the phase diagram of Figure 14, one for reducing and one for oxidizing conditions, related to oxygen fugacities corresponding to QFM and QFM+2 at dry conditions, respectively. In the chosen primitive system, orthopyroxene always crystallizes late, with the potential to produce typically interstitial growth. Earlier orthopyroxene crystallization can be expected at the chosen low pressure only by a significant increase of silica activity of the system.

Acknowledgments

[55] We acknowledge the support of the Universities of Montpellier and Hannover, of the CNRS, and of the European PROCOP program as well as the friendly cooperation established in Oman with the Directorate of Minerals of the MCI. The manuscript has been largely improved thanks to the constructive and patient reviews by Laurence Coogan and Nick Hayman as well as by the Editor, Vincent Salters. We are also grateful to Vincent Salters for his support.

References

Adachi, Y., and S. Miyashita (2003), Geology and petrology of the plutonic complexes in the Wadi Fizh area: Multiple magmatic events and segment structure in the northern Oman ophiolite, *Geochem. Geophys. Geosyst.*, *4*(9), 8619, doi:10.1029/2001GC000272.

Alt, J. C., et al. (1993), *Proceedings of the Ocean Drilling Program, Initial Reports*, vol. 148, Ocean Drill. Program, College Station, Tex.

Alt, J. C., et al. (1996), Hydrothermal alteration of a section of upper oceanic crust in the eastern equatorial Pacific: A synthesis of results from Site 504 (DSDP Legs 69, 70, and 83, and ODP Legs 111, 137, 140, and 148.), *Proc. Ocean Drill. Program Sci. Results*, *148*, 417–434.

Ariskin, A. A. (1999), Phase equilibria modeling in igneous petrology: Use of COMAGMAT model for simulating fractionation of ferro-basaltic magmas and the genesis of high-alumina basalt, *J. Volcanol. Geotherm. Res.*, *90*, 115–162, doi:10.1016/S0377-0273(99)00022-0.

Bach, W., B. Peucker-Ehrenbrink, S. R. Hart, and J. S. Blusztajn (2003), Geochemistry of hydrothermally altered oceanic crust: DSDP/ODP Hole 504B — Implications for seawater-crust exchange budgets and Sr- and Pb-isotopic evolution of the mantle, *Geochem. Geophys. Geosyst.*, *4*(3), 8904, doi:10.1029/2002GC000419.

Berndt, J., C. Liebske, F. Holtz, M. Freise, M. Nowak, D. Ziegenbein, D. Hurkuck, and J. Koepke (2002), A combined rapid-quench and H_2-membrane setup for internally heated pressure vessels: Description and application for water solubility in basaltic melts, *Am. Mineral.*, *87*, 1717–1726.

Berndt, J., J. Koepke, and F. Holtz (2005), An experimental investigation of the influence of water and oxygen fugacity on differentiation of MORB at 200 MPa, *J. Petrol.*, *46*, 135–167, doi:10.1093/petrology/egh066.

Bezos, A., and E. Humler (2005), The $Fe^{3+}/\Sigma Fe$ ratios of MORB glasses and their implications for mantle melting, *Geochim. Cosmochim. Acta*, *69*, 711–725, doi:10.1016/j.gca.2004.07.026.

Bosch, D., M. Jamais, F. Boudier, A. Nicolas, J. M. Dautria, and P. Agrinier (2004), Deep and high temperature hydrothermal circulation in the Oman ophiolite- Petrological and isotopic evidence, *J. Petrol.*, *45*(6), 1181–1208, doi:10.1093/petrology/egh010.

Botcharnikov, R. E., J. Koepke, F. Holtz, C. McCammon, and M. Wilke (2005), The effect of water activity on the oxidation and structural state of Fe in a ferro-basaltic melt, *Geochim. Cosmochim. Acta*, *69*, 5071–5085, doi:10.1016/j.gca.2005.04.023.

Boudier, F., M. Godard, and C. Armbruster (2000), Significance of gabbronorite occurrence in the crustal section of the Semail ophiolite, *Mar. Geophys. Res.*, *21*, 307–326, doi:10.1023/A:1026726232402.

Chenevez, J., and A. Nicolas (1997), Crustal feeding in the Oman ophiolite from the top or from the bottom? A thermal and mass balance model, *Geophys. Res. Lett.*, *24*, 1811–1814, doi:10.1029/97GL01681.

Chenevez, J., P. Machetel, and A. Nicolas (1998), Numerical models of magma chambers in the Oman ophiolite, *J. Geophys. Res.*, *103*(B7), 15,443–15,455, doi:10.1029/98JB00597.

Collier, J. S., and S. C. Singh (1997), Detailed structure of the top of the melt body beneath the East Pacific Rise at 9°40′N

from waveform inversion of seismic reflection data, *J. Geophys. Res.*, *102*(B9), 20,287–20,304, doi:10.1029/97JB01514.

Coogan, L. A. (2003), Contaminating the lower crust in the Oman ophiolite, *Geology*, *31*(12), 1065–1068, doi:10.1130/G20129.1.

Coogan, L. A., R. N. Wilson, K. M. Gillis, and C. J. MacLeod (2001), Near-solidus evolution of oceanic gabbros: Insights from amphibole geochemistry, *Geochim. Cosmochim. Acta*, *65*(23), 4339–4357, doi:10.1016/S0016-7037(01)00714-1.

Coogan, L. A., N. C. Mitchell, and M. J. O'Hara (2003), Roof assimilation at fast spreading ridges: An investigation combining geophysical, geochemical, and field evidence, *J. Geophys. Res.*, *108*(B1), 2002, doi:10.1029/2001JB001171.

Detrick, R. S., P. Buhl, E. Vera, J. Mutter, J. Orcutt, J. Madsen, and T. Brocher (1987), Multi-channel seismic imaging of a crustal magma chamber along the East Pacific Rise, *Nature*, *326*, 35–41, doi:10.1038/326035a0.

Ernst, W. G., and J. Liou (1998), Experimental phase-equilibrium study of Al- and Ti-contents of calcic amphibole in MORB—A semiquantitative thermobarometer, *Am. Mineral.*, *83*, 952–969.

Feig, S. T., J. Koepke, and J. E. Snow (2006), Effect of water on tholeiitic basalt phase equilibria: An experimental study under oxidizing conditions, *Contrib. Mineral. Petrol.*, *152*(5), 611–638, doi:10.1007/s00410-006-0123-2.

Garel, E., O. Dauteuil, and Y. Lagabrielle (2002), Deformation processes at fast to ultra-fast oceanic spreading axes: Mechanical approach, *Tectonophysics*, *346*(3–4), 223–246, doi:10.1016/S0040-1951(01)00280-3.

Ghiorso, M. S., and R. O. Sack (1995), Chemical mass transfer in magmatic processes. IV. A revised and internally consistent thermodynamic model for the interpolation and extrapolation of liquid-solid equilibria in magmatic systems at elevated temperatures and pressures, *Contrib. Mineral. Petrol.*, *119*, 197–212, doi:10.1007/BF00307281.

Gillis, K. M. (2002), The root zone of an ancient hydrothermal system exposed in the Troodos ophiolite, Cyprus, *J. Geol.*, *110*, 57–74, doi:10.1086/324205.

Gillis, K. M., and L. A. Coogan (2002), Anatectic migmatites from the roof of an ocean ridge magma chamber, *J. Petrol.*, *43*(11), 2075–2095, doi:10.1093/petrology/43.11.2075.

Gillis, K. M., and M. D. Roberts (1999), Cracking at the magma-hydrothermal transition: Evidence from the Troodos ophiolite, Cyprus, *Earth Planet. Sci. Lett.*, *169*, 227–244, doi:10.1016/S0012-821X(99)00087-4.

Gregory, R. T., and H. P. J. Taylor (1981), An oxygen isotope profile in a section of Cretaceous oceanic crust, Samail ophiolite, Oman: Evidence for $\delta^{18}O$ buffering of the oceans by deep (>5 km) seawater-hydrothermal circulation at mid-ocean ridges, *J. Geophys. Res.*, *86*, 2737–2755, doi:10.1029/JB086iB04p02737.

Harding, A. J., J. A. Orcutt, M. E. Kappus, E. E. Vera, J. C. Mutter, P. Buhl, R. S. Detrick, and T. M. Brocher (1989), Structure of young oceanic crust at 13°N on the East Pacific Rise from expanding spread profiles, *J. Geophys. Res.*, *94*(B9), 12,163–12,196, doi:10.1029/JB094iB09p12163.

Holland, T. J. B., and J. Blundy (1994), Non-ideal interactions in calcic amphiboles and their bearing on amphibole-plagioclase thermometry, *Contrib. Mineral. Petrol.*, *116*, 433–447, doi:10.1007/BF00310910.

Holtz, F., H. Behrens, D. B. Dingwell, and W. Johannes (1995), Water solubility in haplogranitic melts: Compositional, pressure and temperature dependence, *Am. Mineral.*, *80*, 94–108.

Hooft, E. E. E., R. S. Detrick, and G. M. Kent (1997), Seismic structure and indicators of magma budget along the southern East Pacific Rise, *J. Geophys. Res.*, *102*(B12), 27,319–27,340, doi:10.1029/97JB02349.

Jousselin, D., A. Nicolas, and F. Boudier (1998), Detailed mapping of a mantle diapir below a paleo-spreading center in the Oman ophiolite, *J. Geophys. Res.*, *103*(B8), 18,153–18,170, doi:10.1029/98JB01493.

Juteau, T., M. Beurrier, R. Dahl, and P. Nehlig (1988), Segmentation at a fossil spreading center: The plutonic sequence of the Wadi Haymiliyah area (Haylayn block, Sumail nappe, Oman), *Tectonophysics*, *151*, 167–197, doi:10.1016/0040-1951(88)90245-4.

Juteau, T., D. Bideau, O. Dauteuil, G. Manach, D. D. Naidoo, P. Nehlig, H. Ondreas, M. A. Tivey, K. X. Whipple, and J. R. Delaney (1995), A submersible study in the western Blanco Fracture Zone, NE Pacific: Structure and evolution during the last 1.6 Ma, *Mar. Geophys. Res.*, *17*(5), 399–430, doi:10.1007/BF01371786.

Karson, J. A., S. D. Hurst, and P. Lonsdale (1992), Tectonic rotations of dikes in fast-spread oceanic crust exposed near Hess Deep, *Geology*, *20*, 685–688, doi:10.1130/0091-7613(1992)020<0685:TRODIF>2.3.CO;2.

Karson, J. A., M. A. Tivey, and J. R. Delaney (2002a), Internal structure of uppermost oceanic crust along the Western Blanco Transform Scarp: Implications for subaxial accretion and deformation at the Juan de Fuca Ridge, *J. Geophys. Res.*, *107*(B9), 2181, doi:10.1029/2000JB000051.

Karson, J. A., et al. (2002b), Structure of uppermost fast-spread oceanic crust exposed at the Hess Deep Rift: Implications for subaxial processes at the East Pacific Rise, *Geochem. Geophys. Geosyst.*, *3*(1), 1002, doi:10.1029/2001GC000155.

Kent, G. M., et al. (2000), Evidence from three-dimensional seismic reflectivity images for enhanced melt supply beneath mid-ocean-ridge discontinuities, *Nature*, *406*(6796), 614–618, doi:10.1038/35020543.

Koepke, J., S. T. Feig, J. Snow, and M. Freise (2004), Petrogenesis of oceanic plagiogranites by partial melting of gabbros: An experimental study, *Contrib. Mineral. Petrol.*, *146*, 414–432, doi:10.1007/s00410-003-0511-9.

Koepke, J., S. Feig, and J. Snow (2005a), Late stage magmatic evolution of oceanic gabbros as a result of hydrous partial melting: Evidence from the Ocean Drilling Program (ODP) Leg 153 drilling at the Mid-Atlantic Ridge, *Geochem. Geophys. Geosyst.*, *6*, Q02001, doi:10.1029/2004GC000805.

Koepke, J., S. T. Feig, and J. Snow (2005b), Hydrous partial melting within the lower oceanic crust, *Terra Nova*, *17*, 286–291, doi:10.1111/j.1365-3121.2005.00613.x.

Lagabrielle, Y., and M. H. Cormier (1999), Formation of large summit troughs along the East Pacific Rise as collapse calderas: An evolutionary model, *J. Geophys. Res.*, *104*(B6), 12,971–12,988, doi:10.1029/1999JB900015.

Lippard, S. J., A. W. Shelton, and I. G. Gass (1986), *The Ophiolite of Northern Oman*, *Geol. Soc. Mem. 11*, 178 pp., Blackwell Sci., Malden, Mass.

MacLeod, C. J., and D. A. Rothery (1992), Ridge axial segmentation in the Oman ophiolite: Evidence from along-strike variations in the sheeted dyke complex, in *Ophiolites and Their Modern Analogues*, edited by L. M. Parson, B. J. Murton, and P. Browning, *Geol. Soc. Spec. Publ.*, *60*, 39–63.

MacLeod, C. J., and G. Yaouancq (2000), A fossil melt lens in the Oman ophiolite: Implications for magma chamber processes at fast spreading ridges, *Earth Planet. Sci. Lett.*, *176*, 357–373, doi:10.1016/S0012-821X(00)00020-0.

Manning, C. E., P. E. Weston, and K. I. Mahon (1996), Rapid high-temperature metamorphism of East Pacific Rise gab-

bros from Hess deep, *Earth Planet. Sci. Lett.*, *144*(1–2), 123–132, doi:10.1016/0012-821X(96)00153-7.

Manning, C. E., C. J. MacLeod, and P. E. Weston (2000), Lower-cracking front at fast-spreading ridges: Evidence from the East Pacific Rise and the Oman ophiolite, in *Ophiolites and Oceanic Crust: New Insights From Field Studies and the Ocean Drilling Program*, *Spec. Pap. Geol. Soc. Am.*, *349*, 261–272.

Ministry of Petroleum and Minerals (1986), Geological map of the Sultanate of Oman, scale 1:100,000, Dir. Gen. of Miner., Muscat.

Ministry of Petroleum and Minerals (1992), Geological map of the Sultanate of Oman, scale 1:250,000, Dir. Gen. of Miner., Muscat.

Miyashita, S., Y. Adachi, and S. Umino (2003), Along-axis magmatic system in the northern Oman ophiolite: Implications of compositional variation of the sheeted dike complex, *Geochem. Geophys. Geosyst.*, *4*(9), 8617, doi:10.1029/2001GC000235.

Nehlig, P., T. Juteau, V. Bendel, and J. Cotten (1994), The root zone of oceanic hydrothermal systems: Constraints from the Samail ophiolite (Oman), *J. Geophys. Res.*, *99*(B3), 4703–4713, doi:10.1029/93JB02663.

Nicolas, A., and F. Boudier (1991), Rooting of the sheeted dike complex in the Oman ophiolite, in *Ophiolite Genesis and Evolution of the Oceanic Lithosphere*, edited by T. Peters, A. Nicolas, and R. G. Coleman, pp. 39–54, Kluwer Acad., Dordrecht, Netherlands.

Nicolas, A., and F. Boudier (1995), Mapping oceanic ridge segments in Oman ophiolites, *J. Geophys. Res.*, *100*(B4), 6179–6197, doi:10.1029/94JB01188.

Nicolas, A., and D. Mainprice (2005), Burst of high-temperature seawater injection throughout accreting oceanic crust: A case study in Oman ophiolite, *Terra Nova*, *17*, 326–330, doi:10.1111/j.1365-3121.2005.00617.x.

Nicolas, A., I. Reuber, and K. Benn (1988), A new magma chamber model based on structural studies in the Oman ophiolite, *Tectonophysics*, *151*, 87–105.

Nicolas, A., F. Boudier, B. Ildefonse, and E. Ball (2000), Accretion of Oman and United Arab Emirates ophiolite: Discussion of a new structural map, *Mar. Geophys. Res.*, *21*, 147–179, doi:10.1023/A:1026769727917.

Nicolas, A., D. Mainprice, and F. Boudier (2003), High-temperature seawater circulation throughout crust of oceanic ridges: A model derived from the Oman ophiolites, *J. Geophys. Res.*, *108*(B8), 2371, doi:10.1029/2002JB002094.

Pallister, J. S., and C. A. Hopson (1981), Samail Ophiolite Plutonic Suite: Field relations, phase variation, cryptic variation and layering, and a model of a spreading ridge magma chamber, *J. Geophys. Res.*, *86*(B4), 2593–2644, doi:10.1029/JB086iB04p02593.

Quick, J. E., and R. P. Denlinger (1993), Ductile deformation and the origin of layered gabbro in ophiolites, *J. Geophys. Res.*, *98*, 14,015–14,027.

Rothery, D. A. (1983), The base of a sheeted dyke complex, Oman ophiolite: Implications for magma chambers at oceanic spreading axes, *J. Geol. Soc. London*, *140*, 287–296, doi:10.1144/gsjgs.140.2.0287.

Singh, S. C., G. M. Kent, J. S. Collier, A. J. Harding, and J. A. Orcutt (1998), Melt to mush variations in crustal magma properties along the ridge crest at the southern East Pacific Rise, *Nature*, *394*(6696), 874–878, doi:10.1038/29740.

Singh, S. C., et al. (2006), Seismic reflection images of the Moho underlying melt sills at the East Pacific Rise, *Nature*, *442*, 287–290, doi:10.1038/nature04939.

Stakes, D. S., and H. P. Taylor (1992), The Northern Samail Ophiolite: An oxygen isotope, microprobe and field study, *J. Geophys. Res.*, *97*, 7043–7080, doi:10.1029/91JB02743.

Teagle, D. A. H., J. C. Alt, S. Umino, S. Miyashita, N. R. Banerjee, D. S. Wilson, and the Expedition 309/312 Scientists (2006), Superfast Spreading Rate Crust 2 and 3, *Proc. Integr. Ocean Drill. Program*, *309/312*, doi:10.2204/iodp.proc.309312.2006.

Umino, S., S. Miyashita, F. Hotta, and Y. Adachi (2003), Along-strike variation of the sheeted dike complex in the Oman Ophiolite: Insights into subaxial ridge segment structures and the magma plumbing system, *Geochem. Geophys. Geosyst.*, *4*(9), 8618, doi:10.1029/2001GC000233.

Wilson, D. S., et al. (2006), Drilling to gabbro in intact ocean crust, *Science*, *312*(5776), 1016–1020, doi:10.1126/science.1126090.